AD-A137 664 A STUDY OF LOW LEVEL LASER RETINAL DAMAGE(U) JOHNS 1/1
HOPKINS UNIV LAUREL MD APPLIED PHYSICS LAB
B F HOCHHEIMER 01 FEB 84 N00024-83-C-5301

UNCLASSIFIED F/G 6/18 NL

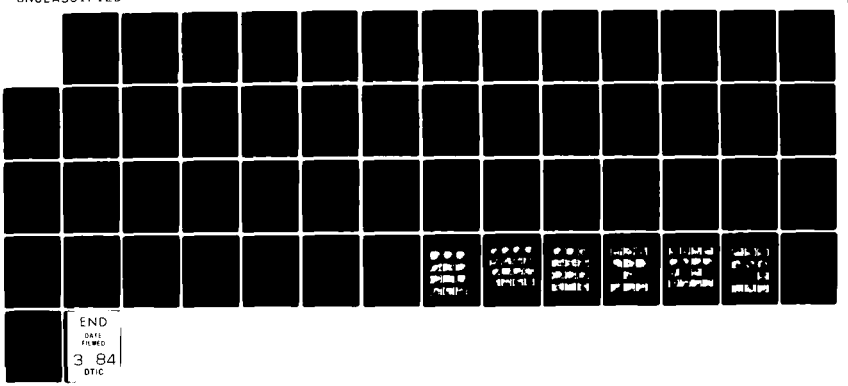

END
DATE FILMED
3 84
DTIC

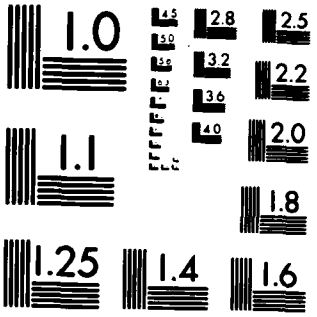

AD

ANNUAL

PROGRESS REPORT

for

U.S. ARMY MEDICAL RESEARCH AND DEVELOPMENT COMMAND
Fort Detrick, Frederick, Maryland 21701

from

RC-RCS-036
The Johns Hopkins University
Applied Physics Laboratory
Johns Hopkins Road
Laurel, Maryland 20707

on

# A STUDY OF LOW LEVEL LASER RETINAL DAMAGE

Approved for public release; distribution unlimited.

B. F. Hochheimer

February 1, 1984



The findings in this report are not to be construed as an official Department of the Army position unless so designated by other authorized documents.

AD

# ANNUAL

# PROGRESS REPORT

for

U.S. ARMY MEDICAL RESEARCH AND DEVELOPMENT COMMAND
Fort Detrick, Frederick, Maryland 21701

from

RC-RCS-036
The Johns Hopkins University
Applied Physics Laboratory
Johns Hopkins Road
Laurel, Maryland 20707

on

## A STUDY OF LOW LEVEL LASER RETINAL DAMAGE



B. F. Hochheimer

February 1, 1984

SECURITY CLASSIFICATION OF THIS PAGE (When Data Entered)

| REPORT DOCUMENTATION PAGE | | READ INSTRUCTIONS BEFORE COMPLETING FORM |
|---|---|---|
| 1. REPORT NUMBER<br>RC-RCS-036 | 2. GOVT ACCESSION NO.<br>AD-A137664 | 3. RECIPIENT'S CATALOG NUMBER |
| 4. TITLE (and Subtitle)<br>A Study of Low Level Laser Retinal Damage | | 5. TYPE OF REPORT & PERIOD COVERED<br>Annual Progress Report<br>2/1/83-1/31/84<br>6. PERFORMING ORG. REPORT NUMBER |
| 7. AUTHOR(s)<br>Bernard F. Hochheimer | | 8. CONTRACT OR GRANT NUMBER(s)<br>N00024-83-C-5301 |
| 9. PERFORMING ORGANIZATION NAME AND ADDRESS<br>The Johns Hopkins University<br>Applied Physics Laboratory<br>Johns Hopkins Road, Laurel, Maryland 20707 | | 10. PROGRAM ELEMENT, PROJECT, TASK AREA & WORK UNIT NUMBERS |
| 11. CONTROLLING OFFICE NAME AND ADDRESS<br>U.S. Army Medical Research & Development Command<br>Fort Detrick, Maryland | | 12. REPORT DATE<br>February 1, 1984<br>13. NUMBER OF PAGES<br>55 |
| 14. MONITORING AGENCY NAME & ADDRESS(if different from Controlling Office)<br>Non-Ionizing Radiation Division<br>Letterman Army Institute of Research<br>Presidio of San Francisco, California 94129 | | 15. SECURITY CLASS. (of this report)<br>Unclassified<br>15a. DECLASSIFICATION/DOWNGRADING SCHEDULE |

16. DISTRIBUTION STATEMENT (of this Report)

Approved for public release; distribution unlimited.

17. DISTRIBUTION STATEMENT (of the abstract entered in Block 20, if different from Report)

18. SUPPLEMENTARY NOTES

19. KEY WORDS (Continue on reverse side if necessary and identify by block number)

Laser Retinal Damage

20. ABSTRACT (Continue on reverse side if necessary and identify by block number)

The general objective of this program is to document changes in the retina due to very low laser irradiation. We have two primary aims. One is to develop and improve methods that can be used, in vivo, to objectively determine changes that occur in the retina from laser irradiation. The second is to determine the mechanisms that cause these retinal changes.

During this past year we have: →

DD FORM 1 JAN 73 1473 EDITION OF 1 NOV 65 IS OBSOLETE

SECURITY CLASSIFICATION OF THIS PAGE (When Data Entered)

(1) Measured the change in retinal reflectivity during YAG and Argon Ion laser burn periods.

(2) Determined the fluorescence decay time of fluorescein dye in water, blood and monkey retinas.

(3) Obtained estimates of the amount of scattered light in the eye in the green and red spectral regions.

DISTRIBUTION:

Commander
U.S. Army Medical Research and Development Command
ATTN: SGRD-RMS
Fort Detrick, Frederick, Maryland 21701
4 copies

Defense Documentation Center (DDC)
ATTN: DDC-TCA
Cameron Station
Alexandria, Virginia 22314
12 copies

Superintendent
Academy of Health Sciences, U.S. Army
Fort Sam Houston, Texas 78234
1 copy

Dean, School of Medicine
Uniformed Services University of Health Sciences
Office of the Secretary of Defense
4301 Jones Bridge Road
Bethesda, Maryland 20014
1 copy

Commander
Letterman Army Institute of Research
ATTN: SGRD-ULZ-RCM/Dr. Neville
Presidio of San Francisco, California 94129
6 copies

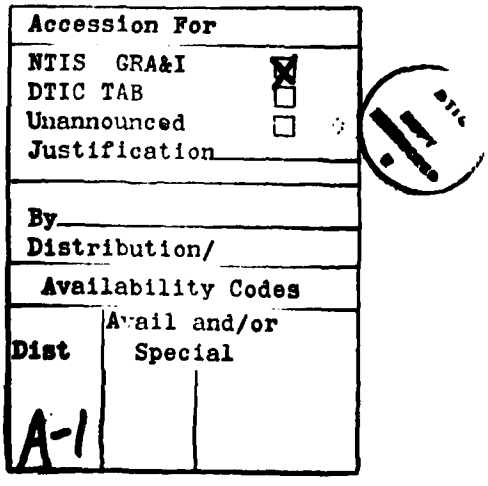

FORWARD

In conducting the research described in this report, the investigator(s) adhered to the "Guide for Laboratory Animal Facilities and Care," as promulgated by the Committee on the Guide for Laboratory Animal, Resources, National Academy of Sciences-National Research Council.

TABLE OF CONTENTS

# CHANGES IN RETINAL REFLECTIVITY DUE TO A LASER BURN

## Introduction

The objectives of this part of the program are:

1. To detect and quantify the subtle clouding effect seen at the retina with low level gallium arsenide laser irradiation.

2. To determine if measurements of retinal reflectivity during laser irradiation will aid in an understanding of low level laser damage mechanisms.

3. To determine the optimum wavelength(s) to use to detect laser retinal damage several days to months after the damage has occurred.

## Methods

A modified fundus camera is used to illuminate a small area of the retina with light from a fiber optics light source. Energy from either a YAG or Argon Ion laser is introduced into the light collection optics by a dichroic beam splitter. The laser light goes through the camera focusing lenses and is sharply imaged on the retina at the center of the fiber optics illuminated area. The reflected energy from the retina is imaged at an iris diaphram which is located at the retinal image over the same area as the fiber optics source. Light going from the aperture goes through a rotating variable wavelength interference filter monochromator and then to a S-20 response photomultiplier tube. The PMT signal is amplified by a digital voltmeter. Data is collected and analyzed by a HP9845B computer. The computer also controls a stepper motor which rotates the filter monochromator.

With this system, a reflection spectra of the retina can be recorded at 20 wavelengths from 400 to 1200 nm in 5.3 seconds. The S-20 PMT has little sensitivity above 800 nm but can be replaced with a S-1 response tube if it is desirable. It is also possible to pulse the laser on and off and record reflection data only when the laser is off.

## Results

### A. YAG Laser Burns

In Table I are shown the results from five YAG laser burn measurements of retinal reflectivity. The CW YAG laser power at the cornea is approximately 50 milliwatts multimode. Tests 1, 3 and 5 were made with full intensity; Test 2 with a neutral density filter of 0.15 in the laser beam; and Test 5 with a 0.3 neutral density filter. In Test 5, no laser burn could be

TABLE I

1. Laser on 121 Seconds, Full Intensity

| λ | % Increase in retinal reflectivity |
|---|---|
| 462 | 78 |
| 540 | 70 |
| 658 | 60 |
| 695 | 53 |

2. Laser on 303 Seconds, Full Intensity with ND 0.15

| λ | % Increase in retinal reflectivity |
|---|---|
| 462 | 22 |
| 540 | 28 |
| 658 | 16 |
| 695 | 22 |

3. Laser on 191 Seconds, Full Intensity (Graphs are shown for this data)
(Laser on 63 to 254 seconds)

| λ | % Increase in retinal reflectivity |
|---|---|
| 462 | 92 |
| 540 | 107 |
| 658 | 67 |
| 695 | 48 |

4. Laser on 300 Seconds, Full Intensity

| λ | % Increase in retinal reflectivity |
|---|---|
| 462 | 116 |
| 540 | 150 |
| 658 | 89 |
| 695 | 69 |

5. Laser on 307 Seconds, Full Intensity ND 0.3

No change in any wavelength

seen; and there was no detectable change in retinal reflectivity at any wavelength. Although the laser power level is not well known, a reduction in power level by a factor of two will not produce ophthalmoscopically visible retinal damage.

With full intensity, the reflectivity increases with an increase in irradiation time; and the greatest increase is at the shorter wavelengths. Data is not recorded past 700 nm because of a filter in the detector light path to remove the 1.06 micron laser energy. With the neutral density 0.15 filter, the increase in reflectivity is reduced by about a factor of five times from the full intensity burns (compare Test 2 and 4).

The data recordings for Test 3 are shown in Figure 1. One hundred and fifty spectral scans were recorded with a ten second delay between scans. Our computer storage limits the total number of scans to less than 200 so that even though a single scan takes only 5.3 seconds a time delay between scans is necessary if a long recording time is desirable. The laser was turned on from 63 to 254 seconds, a 191 second burn period. An inspection of the curves in Figure 1 shows that the retinal reflectivity did not increase until approximately 100 seconds, that is 40 seconds after the laser was turned on. The peak increase in reflectivity occurs at approximately 250 seconds, the time the laser was turned off. From that time until the end of the test, 2370 seconds, almost 40 minutes, there is a gradual decrease in reflectivity.

B. Argon Ion Laser Burns

Argon ion laser retinal burns were made using the 488 nm line in a manner similar to that used for the YAG laser burns except that a 515 nm long pass filter was used in the detector light path to remove reflected laser light. Figure 2 is the first sheet from the computer. It records the initial data including the voltage signal levels and reflectivity of the standard reflector. The standard reflector is Kodak White Reflectance Standard and a neutral density 1.0 filter. Standard reflection signals of less than 0.045 are due to residual dark current in the PMT. The time at the end of each scan is recorded. The number after the scan time is the voltage recorded for 500 nm; this is used as a check on system performance during a test. Table II shows the wavelengths at which data is recorded. For the test run indicated in Figure 2, the laser was on from 26.5 to 111.3 seconds at a power level sufficient to produce a definite burn. The wavelength data is plotted as shown in Figure 3A. The data point at 200 units is the cross over from one half of the interference monochromator to the other half and not a good point. Figure 3B is at 106 seconds when the laser is on and indicates a high degree of retinal fluorescence. Figures 4A and 4B are after the laser was turned off. Specific wavelength data is plotted as shown in Figures 5 and 6. Figure 5A is at 462 nm and not useful because of the 515 nm long pass filter. Figure 5B shows the data at 540 nm. Before the laser is turned on, the retinal reflectivity is approximately 11 percent; during the laser burn, the fluorescence swamps out the signal; after the laser burn, the reflectivity has risen to 17 percent and slowly decreases to 15 percent at 1000 seconds after the burn. Figure 6 shows similar data for 658 and 760 nm.

We can also pulse the laser on and off with a Uniblitz shutter and record reflectance data when the laser is off thereby avoiding the fluorescence problem. In the previous continuous maximum power test, the laser was on for 191 seconds. In a series of pulse tests, the laser was on for 90 seconds in 1.0 second bursts every 5.4 seconds. The data is similar at high power to the continuous burns. With the laser power level reduced by 25

TABLE II

| Data Point Number | Wavelength nm | Standard Signal level, volts | |
|---|---|---|---|
| 1 | 345 | 0.04087 | NG |
| 2 | 384 | 0.04372 | |
| 3 | 423 | 0.04846 | |
| 4 | 462 | 0.05099 | |
| 5 | 501 | 0.10528 | |
| 6 | 540 | 0.93819 | |
| 7 | 579 | 0.98578 | |
| 8 | 618 | 0.93477 | |
| 9 | 658 | 0.82208 | |
| 10 | 697 | 0.55451 | |
| 11 | NG | 0.05101 | NG |
| 12 | 757 | 1.09997 | |
| 13 | 820 | 0.29215 | |
| 14 | 882 | 0.06659 | ? |
| 15 | 940 | 0.04281 | |
| 16 | 1002 | 0.04667 | |
| 17 | 1065 | 0.04202 | NG |
| 18 | 1127 | 0.04061 | |
| 19 | 1190 | 0.04363 | |
| 20 | 345 | 0.04511 | |

times, pulsed mode, the data in Figure 7 was recorded. The 515 nm long pass filter was removed. At 462, 540, 658 and 695 nm, a slight rise in reflectivity can be detected. The laser pulse time was from 21.3 to 467 seconds.

We alsc plot the data from a given scan minus the average value up to that time. This type of plot shows the trend of the data; if the trend is positive, the values are increasing. In general, the trend plots, Figure 8, show a constantly increasing reflectivity. At 540 nm, the increase is small near 200 seconds; but it is still positive. At 695 nm, the increase is approximately zero until after 200 seconds when it increases. These curves show that although the initial and final values are almost identical for all wavelengths these values are not arrived at in the same way.

This pulsed energy did not produce a retinal burn visible immediately after the test, but one was just visible one hour later. A change in reflectivity could be recorded at the time when a burn could not yet be seen.

This test produced 200 spectral scans, the data for all wavelengths is printed out for every fifth scan as shown in Figure 9. The first row of numbers is the scan number, the second row the reflectivity at $\lambda_1$, the third row at $\lambda_2$, etc. This order is repeated for every set of numbers. As an example, the fifth row of numbers in the first set are the

reflectivity values for 462 nm. The initial value is 8.5 percent; it rises to 10.2 percent at the 71st scan, decreases somewhat for scans 101 to 126 and gradually rises to 10.5 percent at scan 196.

### C. Retinal Fluorescence

As noted above, we found a high degree of retinal fluorescence. Since all of our monkeys have had one or more fluorescein angiograms, we do not know if the fluorescence is due to residual fluorescein.

The spectra of this retinal fluorescence due to 488 nm laser light was recorded with continuous illumination. The 515 nm long pass filter was used to remove the laser light; this distorts the spectral shape of the fluorescence.

Figure 10 is the recorded spectra; the Y-axis should read relative intensity. No correction for instrument transmission is included. Taking into consideration the influence of the 515 nm filter, this spectra could be due to fluorescein.

Figure 11 is the time history of the fluorescence for 462, 540, 658 and 695 nm. Because of the filter, there is no energy at 462 nm. In the remaining time histories, there is a rapid rise in fluorescence to a peak value, a rapid decay and a slow decay to a constant value. The high peak rise seems to disappear if the retina is not burned. In this case, the signal to noise ratio in the recorded energy values is low; therefore, there is some uncertainty in this. In Figure 11, the dotted curves are the originally recorded data, and the solid curves are running averages over five points.

### D. Photographic Records

One eye of a monkey had a series of eight burns placed on his retina with the 488 nm line of the Argon Ion laser. Power levels were varied over a factor of 25 times in making these burns. Fundus photographs were taken at 450 to 850 nm in 50 nm steps at various times after retinal exposure. This series and the times after exposure are shown in Figure 12. The retinal burns are most apparent at short wavelengths immediately after exposure and at red (600-650 nm) several days later. At no time are they most visible in the near infrared.

## Problem Areas

### A. Locating Old Burns

We wished to photoelectrically record the reflectivity of the retina at laser burn areas for long post-irradiation times. Unless the burn is very severe, a healing process takes place; and we can no longer see the

burns with our fundus camera. Since the laser retinal burns are very small, approximately 50 microns in diameter, the fiber optics illumination used for reflectivity measurements must be positioned with high accuracy. This cannot be done unless the burns can be seen. Because of this, the reflectivity can not be measured at long post-exposure times.

B. Computer Data Collection

One of the problems in using a computer to collect data is that there is often an overabundance of data. We have not yet had enough time to analyze all of our retinal reflectivity data. A second unresolved problem is the proper format to display the results. We are getting better at this.

C. Equipment Reliability

As our experiments are becoming more sophisticated, the equipment used is more complex. For many of our tests, we could not measure the laser power at the eye because our Laser Precision Power Meter was being repaired. During the past year, the Princeton Applied Research signal averager and the Hewlett-Packard computer have needed factory repairs. The Hewlett-Packard multiprogrammer used to operate stepper motors and do analog to digital conversion is now at the factory for repair. Because of this problem, we are making redundant measurements as often as possible.

## Conclusions

1. Changes in retinal reflectivity can be detected photoelectrically at levels below those that can be observed visually.

2. With continuous wave YAG laser energy, it is difficult to observe near threshold retinal lesions because the energy difference necessary to make a highly visible burn and that which will make no burn is very small.

3. For detection of old retinal laser-induced lesions, a monochromatic series of retinal photographs covering the range from 400 to 800 nm is the method we recommend. This question will be considered further in the section on future efforts.

4. I have replotted the data for the pulsed Argon Ion laser test shown in Figure 9. The retinal reflectivity is plotted in Figure 13 to show the increase with time and wavelength. Plotted is data for the 1st scan, before irradiation; the 61st scan, almost at the end of the irradiation period; and the 196th scan, at the end of the data collection period.

   There is a rather constant increase in reflectivity at all wavelengths shorter than 800 nm. The data at 882 is plotted but

may not be reliable. If it is assumed that different retinal layers can be seen with variations in wavelength, deeper layers are seen at longer wavelengths, then this plot might indicate that all layers of the retina above the choriocapillaries are being equally damaged. I think it is more likely that the pigment epithelium is being damaged and there is a white layer of edema formed that is transparent at 800 nm.

## STRAY LIGHT IN THE EYE

### Measurement of Scattered Light

In last year's progress report, we showed that if a very small area of the retina is directly illuminated the total amount of light impinging on the rest of the retina may be between one-half to over ten times the directly illuminated power. A small area of retina was illuminated, and the directly reflected light was compared to the light coming from a similar area of the retina some distance away from the directly illuminated area. In the visible spectral region, the nonilluminated area at six degrees from the illuminated area reflected approximately 1/500 of the energy from the illuminated area. At 750 nm, this ratio is 1/50 and at 800 nm 1/10. In the visible spectrum, our data agrees very well with other published data. The ratio of illuminated area to nonilluminated area of the retina was approximately $10^{-4}$.

This stray light in the eye is composed of light scattered by the cornea, aqueous, lens and vitreous; by light reflected many times by the retina; and by light internally scattered in the choroid and sclera. An expression for the reflected light term was derived using simple geometry and assuming a diffuse retina. The derived expression indicated that only a very small amount of light should be internally reflected even for very high values of retinal reflectivity. Even if the retina is 100 percent reflecting, the internal reflected energy per unit area would only approach the ratio of illuminated to nonilluminated area.

From our experiments that measured the increase in reflectivity of the retina when it is burned with a high energy laser beam, we knew that the retinal reflectivity could be increased by almost a factor of two for wavelengths from 500 to 800 nm. Using this fact, we can deduce some information on the percentage of light scattered in the eye.

If the retinal reflectivity is $R_1$ for a nonburned area, $R_2$ for a burned area and the amount of scattered light is S, then the directly reflected energy E measured from nonburned area is

$$E_1 = KR_1(1 - S)^2 \qquad (1)$$

where K is a nondefined constant. The directly reflected energy measured from the burned area is

$$E_2 = KR_2(1 - S)^2. \qquad (2)$$

The ratio of these terms is

$$\frac{E_1}{E_2} = \frac{R_1}{R_2}. \qquad (3)$$

For a nonilluminated area some distance from the laser burn when the burned area is illuminated, the measured reflected energy before the burn will be

$$E_1^1 = K\left(\frac{A}{s}\frac{R_1}{(1 - Y)}(1 - S)^2 + \frac{A}{s}\frac{S(1 - S)}{(1 - Y)}\right). \qquad (4)$$

A/s is the ratio of illuminated to nonilluminated area, Y the area weighted reflectivity and R and S are defined as above. This expression and its derivation is similar to that in last year's progress report with an additional scattering term $S(1 - S)/(1 - Y)$.

When the illuminated area is burned with a laser, its reflectivity will increase, increasing the measured scattered light to a value given by

$$E_2^1 = K\left(\frac{A}{s}\frac{R_2}{(1 - Y)}(1 - S)^2 + \frac{A}{s}\frac{S(1 - S)}{(1 - Y)}\right). \qquad (5)$$

The ratio of equations (4) to (5) is

$$\frac{E_1^1}{E_2^1} = \frac{R_1(1 - S) + S}{R_2(1 - S) + S}.$$

Let

$$\frac{E_1}{E_2} = \frac{1}{C_1} = \frac{R_1}{R_2}$$

or

$$R_2 = C_1 R_1$$

and

$$\frac{E_1^1}{E_2^1} = \frac{1}{C_2}$$

then

$$\frac{1}{C_2} = \frac{R_1(1 - S) + S}{C_1 R_1(1 - S) + S}.$$

$C_1$ and $C_2$ are measured energy ratios on and off the burned areas. Let $R_1 = R$, the retinal reflectivity before being laser burned. S is the amount of scattered light, (1 - S) the energy not scattered that reaches the retina.

Rearranging the terms

$$C_2R(1 - S) + C_2S = C_1R(1 - S) + S$$

$$C_2S - C_2RS + C_1RS - S = C_1R - C_2R$$

$$S = \frac{R(C_1 - C_2)}{(C_2 - 1) + R(C_1 - C_2)}.$$

If $C_1$, $C_2$ and R are known, S can be found.

Using the same optical system described in the section on Retinal Reflectivity, three burns were placed on the retina of a cynomolgus monkey in the region above the macula using the 488 nm line of an argon ion laser for 90 seconds. Although the amount of laser energy is unknown, it was kept at a constant value and the burn time fixed at 90 sec with a Uniblitz shutter. The area to be burned was illuminated with white light. The reflected energy was filtered first with a 515 nm long pass filter to eliminate the laser energy and secondly with a variable wavelength interference filter monochrometer whose bandwidth is 20 nm.

The monochrometer was set at 550 nm, and the reflected energy measured before and after the laser burn. The area used for energy measurements was about one-half the diameter of the laser burn.

The measured values of $C_1$, the energy ratios after the burn to before the burn, are 1.95, 2.40 and 3.04. The reflected light from an area three degrees away from the burn area was then measured for a second set of burns. This second set of burns were just below the first set. The measured values of $C_2$ are 1.19, 1.50 and 1.52. It is apparent that the repeatability is not high.

Similar sets of burns were made with the monochrometer set at 650 and 750 nm. There is insufficient energy to do this at 800 nm. The results are tabulated in Table I.

These values were averaged and values of $(C_1 - C_2)$ and $(C_2 - 1)$ computed. Using what seems to be an appropriate value for retinal reflectivity, the amount of scattered light was found. This is shown in Table II. Values of S were also calculated for higher values of R.

Over this past year, many measurements have been made of the retinal reflectivity of cynomologus monkeys. Using what I believe to be our most reliable sets of data, the reflectivity at 550, 650 and 750 nm were obtained and are listed in Table III.

If the scattered light is as high as it appears to be, the measured values of retinal reflectivity are too low; they should be increased by $1/(1 - S)^2$ where S is taken at a true value of R.

Since our accuracy is not high, one iteration is sufficient. I believe this exercise indicates that the scattered light (cornea-lens-vitreous-aqueous) is high in the visible spectral region 30-40 percent and decreases in the red to 10 percent and that the retinal reflectivity is higher than previously estimated.

This scattering would account for the large value of stray light in the visible but not in the infrared. Since the amount of internally reflected

TABLE I

| $\lambda$ = 550 nm | $C_1$ | $C_2$ |
|---|---|---|
| | 1.95 | 1.19 |
| | 2.40 | 1.50 |
| | 3.04 | 1.52 |
| $\lambda$ = 650 nm | $C_1$ | $C_2$ |
| | 2.36 | 1.43 |
| | 2.36 | 1.31 |
| | 2.38 | 1.46 |
| $\lambda$ = 750 nm | $C_1$ | $C_2$ |
| | 1.65 | 1.33 |
| | 1.49 | 1.36 |
| | 1.65 | 1.50 |

TABLE II

| | | | |
|---|---|---|---|
| $\lambda$ = 550 nm | $C_1 - C_2 = 1.1$ | | |
| | $C_2 - 1 = 0.40$ | | |
| | R = 10% | R = 20% | R = 40% |
| | S = 21% | S = 36% | S = 52% |
| $\lambda$ = 650 nm | $C_1 - C_2 = 0.97$ | | |
| | $C_2 - 1 = 0.40$ | | |
| | R = 15% | R = 30% | R = 60% |
| | S = 26% | S = 42% | S = 59% |
| $\lambda$ = 750 nm | $C_1 - C_2 = 0.20$ | | |
| | $C_2 - 1 = 0.40$ | | |
| | R = 20% | R = 40% | R = 80% |
| | S = 9% | S = 17% | S = 28% |

light is probably low at all wavelengths, the high value of stray light in the red and infrared must be due to light scattered by the choroid and sclera.

Geeraets and Berry (AJO 66, 15, 1968) give spectral absorption curves for monkeys and humans. The monkeys used were rhesus, the cynomolgus we use are much less pigmented. The human data may be more appropriate.

TABLE III

| | 550 nm | 650 nm | 750 nm |
|---|---|---|---|
| | 0.14 | 0.18 | 0.26 |
| | 0.08 | 0.12 | 0.20 |
| | 0.10 | 0.17 | 0.25 |
| | 0.11 | 0.17 | 0.24 |
| | 0.10 | 0.14 | 0.19 |
| Average | 0.106 | 0.156 | 0.228 |

TABLE IV

| $\lambda$ | 550 nm | 650 nm | 750 nm |
|---|---|---|---|
| Measured R | 10% | 15% | 20% |
| Computed S | 21% | 26% | 9% |
| $\left(\frac{1}{1-S}\right)^2$ | 1.6 | 1.8 | 1.2 |
| $R\left(\frac{1}{1-S}\right)^2$ | 16% | 27% | 24% |
| New computed S | 31% | 40% | 11% |

TABLE V

| $\lambda$ nm | % Absorption | $(\text{Transmission})^2$ |
|---|---|---|
| 550 | 75 | 0.06 |
| 650 | 65 | 0.12 |
| 750 | 45 | 0.30 |
| 800 | 35 | 0.42 |

When light hits the choroid, some is transmitted, is reflected by the sclera, is transmitted back through the choroid. If it is assumed that the sclera is almost 100 percent reflecting, then in the red 30 to 40 percent of the light impinging on the retina may be reflected back into the eye.

Table VI is a comparison between our data taken on live monkey eye and the data of Geeraets and Berry for the retinal reflectivity of an enucleated human retina and the data of Boettner and Wolter (Invest. Opthal., 1,776, 1962). These data were taken with different eyes and even different species yet the agreement is fairly good. Our data for scattered light at 650 nm

TABLE VI

| λ | Our Data | | Geeraets & Berry | Boettner & Wolter |
|---|---|---|---|---|
| | % Scattered Light | % Retinal Reflectivity | % Human Retinal Reflectivity | % Scattered Light Optics |
| 550 | 30 | 16 | 12 | 35 |
| 650 | 40 | 27 | 17 | 30 |
| 750 | 10 | 24 | 22 | 26 |

seems to be too high; and since this also effects the reflectivity at that wavelength, it is also high.

## Stray Light at Long Wavelengths

Our previous measurements were taken only at 50 nm intervals from 500 to 800 nm. We wished to both extend the wavelength region and to record data at smaller intervals. In order to do this, we used a two-channel signal averager. White light from our fiber optics source illuminated a small retinal area. The return beam went through a free running rotating interference filter monochrometer. The directly reflected light was stored in channel B and the reflected light three degrees away was stored in channel A. Using an S20 response photomultiplier tube, data was taken from 450 to 825 nm. The ratio of channel A to channel B is the percentage of stray light from the retina corrected for input energy and instrument reponse. This method is excellent for indicating the whole spectral variation; however, many scans are needed for recording the indirectly reflected energy, and long-term drift in DC levels prevent recording absolute values. In addition to this, a zero-level error can produce an unknown tilt in the zero axis. Figure 14 shows the A and B scan and the A/B ratio. In Figure 14, our best estimate of the zero x-axis for the A/B ratio is drawn in. The stray light increases at short wavelengths, shows some structure between 450 and 500 nm, is almost flat to 700 nm and rises quickly from 700 to 825 nm. This is what is expected based on last year's data.

The S20 PMT was replaced with an S1 tube, and the experiment was repeated for the range from 700 to 950 nm. Figure 15 are two A/B ratios using 20 scans. These curves indicate a rapid rise after 700 nm and a level value to 950 nm. In order to determine if the fine structure in these curves are real, a 200 scan recording was made; see Figure 16. The fine structure disappears with sufficient averaging to remove noise.

## Summary

Although much of the data we have obtained this year has low accuracy, it has enabled us to get a much better overall picture of stray light in the

eye. In the visible, the stray light is lowest and almost entirely due to light scattered by the optics of the eye. In the red and near infrared, the scattering decreases but the energy transmitted through the choroid and reflected by the sclera predominates. At all wavelengths, light reflected by the retina, as if the eye acted like an integrating sphere, is negligible.

This stray light does not affect our visual acuity because most of the stray light strikes the retina at high angles of incidence and is very inefficient in evoking any visual response. The Stiles and Crawford effect (B. H. Crawford, Proc. of the Royal Soc., 124, 81, 1938) indicate that light hitting the retina 14 degrees off axis has an efficiency of only 10 percent of that on axis; and the efficiency is falling fast, even on a log plot, for larger angles.

## FLUORESCEIN DYE FLUORESCENCE

### Introduction

The rate of emission of fluorescent light is given by

$$E = I_a \phi_f$$

where $I_a$ = absorbed light

and $\phi_f$ = fluorescence efficiency and is given by

$$\phi_f = K_f/(K_f + K_n + K_g + K_q(Q))$$

where $K_f$ = fluorescence rate constant

$K_n$ = nonradiative rate constant

$K_g$ = triplet state formation rate constant

$K_q$ = quenching rate constant, a function of the amount of quencher (Q).

When the light is turned off, the fluorescence decays with a lifetime $\tau$ where $\tau$ is given by

$$1/\tau = K_f + K_n + K_g + K_q(Q)$$

let $\tau_f$ = radiative lifetime

if $1/\tau_f = K_f$

then $\phi_f = \tau/\tau_f$.

If $\tau_0$ is the lifetime with no quencher and $\phi_f^0$ the efficiency with no quencher, then

$$\tau_0 = 1/\phi_f^0 = 1/(K_f + K_n + K_g)$$

and

$$\phi_f^0/\phi_f = 1 + K_q(Q)/(K_f + K_n + K_g) = 1 + K(Q)$$

where K is generally known as the Stern-Volmer quenching constant or

$$\phi_f^0/\phi_f - 1 = K_q \tau_0[Q] = K(Q);$$

the quenching is given by $\phi_f/\phi_f^0$ or $\tau_0/\tau_f$

$$\text{quenching} = 1/(K(Q) + 1) = 1/(K_q \tau_0(Q) + 1).$$

If the quencher is oxygen, then

$$(Q) = SpO_2$$

where S is the solubility and $pO_2$ the partial pressure of oxygen. $K_q$ is dependent on viscosity (C. A. Parker, PHOTOLUMINESCENCE OF SOLUTIONS, Elsevier Publishing Co., New York, 1968).

In most solutions, oxygen is a very efficient quencher by transfer of triplet state dye energy to the triplet ground state of oxygen forming excited singlet oxygen and a ground state dye molecule. The reaction is diffusion limited and hence the dependence of $K_q$ on viscosity. It is possible to determine the degree of quenching by measuring either the intensity loss or a change in decay time. An intensity loss may also occur if a dye molecule is bound to another molecule with an increase in the nonradiative losses.

We know that the fluorescence intensity of fluorescein in blood is lower than in water by approximately two times. A pyrene dye, which absorbs and fluoresces at the same wavelength as fluorescein, does not show the drop in intensity in blood compared to water (Hochheimer, Exp. Eye Res. 27, 1, 1978). This indicates that blood contains a quencher for fluorescein and the loss in intensity is not due to the absorption of light in blood. This quenching effect for fluorescein can be due to the binding of dye to blood proteins with an increase in nonradiative loss of the excited state or a transfer of energy from the excited state to a second molecule. If the second method predominates, oxygen may be the acceptor molecule.

The most common method used today to measure fluorescence decay times is to use a fast pulse of excitation light and measure the decay of fluorescence directly. If the decay time is not single valued, this method can detect multiple decay times. The modulation-phase detection method that we use assumes a single valued decay time. With the pulse method, high powered pulses must be used; with the modulation method, low average energy can be used. Since the retina is very sensitive to damage from nanosecond pulses of light, we choose to use the modulation-phase shift method.

## Method

In the eye, it is not possible to measure the fluorescence quantum efficiency of a dye; however, it is possible to measure the fluorescence decay time. To do this, the following system was assembled.

A Coherent Radiation Inova 90 Argon Ion Laser emits the 488 nm transition. The laser beam is modulated by an Interacton AOM125H Acoustic-Optic Modulator. The modulator is driven at 20 MHz by an Interacton ME Signal Processor and a Hewlett-Packard 3325A Synthesizer/Function Generator. The moldulated beam laser beam goes through our modified Zeias Fundus Camera to either an animal eye or to a test solution. The fluorescent energy is gathered by the fundus camera optics to an S-20 photomultiplier tube. A Schott 515 nm long pass solid glass filter prevents the laser light from reaching the PMT.

The output of the PMT is amplified by a Princeton Applied Research 5202 high frequency lock-in amplifier. This amplifier has a phase detector option which measures the in-phase and quadrature signals and computes both a phase signal and the signal amplitude. Both signals are recorded on a two-pen strip chart recorder.

If a modulated light beam excites a fluorescent dye, the fluorescence output is also modulated with a phase delay determined by the decay time. This phase shift $\phi$ is given by

$$\tan \phi = 2\pi f \tau$$

where f is the modulation frequency and $\tau$ the decay time (Bailey and Rollefson, J. Chem. Phys. 21, 1315, 1953). With a decay time of $10^{-8}$ seconds and a frequency of 20 MHz, the phase delay is approximately 45 degrees. The degree of modulation of the fluorescent energy decreases as the phase shift increases to zero at a 90 degree phase shift (Spencer and Weber, Ann. of N. Y. Acad. Sci. 158, 361, 1969). At 45 degrees, the phase shift is sensitive to changes in decay time without excessive loss in modulated fluorescence.

## Results

We first measured the decay time in a fluorescein water solution, the fluorescein concentration was $5 \times 10^{-5}$ molar. The measured decay time was $9.82 \times 10^{-9}$ seconds. In order to obtain a zero phase reference signal, a white diffuse reflector is placed at the position of the fluorescein solution and the 515 nm filter removed.

Bailey and Rollefson measured the decay time at this concentration and found it to be about $7.0 \times 10^{-9}$ seconds. In their experiment, the fluorescent energy was collected at 90 degrees to the excitation energy; in our experiment, the collected fluorescent energy is close to 0 degrees from the excitation energy. Multiple internal scattering in the solution would account for the difference. They also show the concentration dependence of the decay time. It varies from $4.6 \times 10^{-9}$ seconds at low concentrations to $7.9 \times 10^{-9}$ seconds at a concentration of $5 \times 10^{-4}$ molar.

The water solution was replaced with a fluorscein-whole blood solution (monkey blood was used), the fluorescein concentration was $5 \times 10^{-5}$ molar, assuming blood to have the same weight as water. Because of differences in weight between blood and water, because some of the fluorescein is bound and because blood contains solids, the molarity in blood is not well defined. The decay time in the fluorescein blood solution was measured to be $8.24 \times 10^{-9}$ seconds.

A variable $CO_2$-$O_2$ gas mixture was injected over the fluorescein-blood solution as it was slowly stirred with a magnetic stirrer. Previous tests indicated that this procedure could be used to change the blood oxygen concentration without visibly changing the blood viscosity. There was no measured change in decay time upon going from 100 percent $O_2$ to 100 percent $CO_2$. Our system can easily detect a $0.1 \times 10^{-9}$ second, the precision seems to be about $0.05 \times 10^{-9}$ second. This result was quite a surprise; we had

expected a large change in decay time with oxygen concentration. There is a slight increase in fluorescein intensity with oxygenation, this is likely due to an increase in transmission.

We next injected a monkey with fluorescein and measured the decay time of the dye in the retina. This decay time did not seem to vary at times longer than several minutes after injection. In a normal nondamaged retinal area, the decay time was found to be $5.63 \times 10^{-9}$ seconds; and on an area previously damaged by a laser, the decay time was $5.04 \times 10^{-9}$ seconds.

A second monkey was given a fluorescein injection, and the fluorescent decay times measured when the animal was breathing pure oxygen and when the endotracheal tube was clamped off for three minutes forcing the animal to increase its $CO_2$ uptake. With 100 percent oxygen, the measured decay time was $5.31 \times 10^{-9}$ seconds; and with the increased $CO_2$ breathing, it was $6.15 \times 10^{-9}$ seconds.

## Discussion

A comparison of some of the fluorescent properties of fluorescein when dissolved in blood and water seems to indicate conflicting evidence. There is a large decrease in intensity in blood. This could be accounted for by quenching reactions. The decay time, however, does not change dramatically nor does it change in blood with a change in $pO_2$. This lack of change in decay time indicates that some of the fluorescein dye molecules are bound in such a way that they no longer contribute to fluorescence. The nonfluorescent fluorescein molecules have either a very acid local environment, or the hydrogen atoms have been stripped away as in an alcoholic solution, or the dye structure is changed as in the change from fluorescein to nonfluorescing phenolphthalein. Either the remaining "nonbound" fluorescein molecules are shielded from $O_2$, or more likely, the $O_2$ is bound to the hemoglobin and the $O_2$ is shielded from the fluorescein.

The fact that blood has little effect on the decay time of fluorescein and is not affected by blood $pO_2$ means that any changes seen in the retina are probably not due to the fluorescein in the animal blood system.

The fluorescence decay time of fluorescein in an animal retina is much shorter than in blood and is even shorter than in a water solution. From previous experiments, the concentration of fluorescein in the retina at some twenty to forty minutes after injection seems to be about $5 \times 10^{-5}$ molar based on the shape of the emission spectra and the local pH is about seven based on the shape of the excitation spectra. The decay time in the retina is also affected by the local oxygen concentration.

These retinal measurements can only be reconciled if there is a high degree of quenching, and the dye molecules are not bound as they are in blood. This is in agreement with fluorescence polarization data from the retina which indicates a low degree of binding.

When fluorescence measurements are taken on a burn-damaged area of the retina, the intensity increases, the polarization decreases and the decay time

decreases. I do not as yet have good excitation and emission spectra for this case.

The intensity and polarization changes indicate an increase of unbound dye; the decay time change indicates an increase in quenching. Any explanation of these changes that occur from a damaged to a nondamaged area of the retina would be very speculative without more information.

When the decay time measurements are incorporated in our main fluorescence program, then all the available fluorescent information can be obtained at the same time on the same animal for both normal and various degrees of light-damaged retina. This data together with the analysis of fluorescence in freeze-dried eyes should give us a better perspective of light damage in the eye.

## FUTURE PLANS

1. Retinal reflection measurements will be made while the retina is being irradiated with a pulsed YAG laser. A transient effect can be seen where the retina appears white for a short period, 5-20 seconds, after the pulsed irradiation. This may be similar to the "clouding" of the retina seen by Lund and Beatrice with a pulsed gallium arsenide laser.

2. A long-term multi-wavelength series of retinal photographs will be made after continuous wave and pulsed YAG burns are made on a monkey retina. Lund (Supplement Invest. Ophth. and Vis. Sci., April 1974, p. 52) reported on a short-term photographic series of gallium arsenide laser burns. His results indicate a considerable difference exists between infrared laser burns and the burns we have documented for argon ion laser burns. We wish to have a longer term followup and do both CW and pulsed burns.

3. We have recently acquired a high brightness xenon arc source and the associated optics and animal holder that enables us to irradiate the retina with sufficient energy to cause a burn in reasonably short time at any wavelength from 400 to 1000 nm. From Ham's work (Ham, Mueller, Ruffolo, Cleary, Clark, Guerry and Guerry, "Biological Applications and Effects of Optical Masers," Army Research Report DADA 17-72-C-2177, 1982), we know the minimum intensity needed to make a retinal lesion in 100 seconds. The intensity will be doubled and 300 micron retinal lesions formed on a monkey retina at 50 nm intervals from 400 to 1000 nm. The time course of these lesions will be followed with monochromatic retinal photography at suitable intervals for the next six months to a year.

4. We will incorporate the fluorescence decay time measurements in our main fluorescence program so that all possible data can be collected from a single animal after one dye injection. Both normal and light-damaged retinal areas will be measured.

5. After a fluorescein dye injection, a monkey eye, with numerous light-induced retinal lesions, has been freeze dried and vacuum embedded with paraffin (Bellhorn, Invest. Ophthal. and Vis. Sci. 19, 870, 1980). These eyes will be sectioned and examined with fluorescence microscopy to determine where the fluorescein seen in angiograms is located.

6. Our analysis of light scatter in the eye is not completely satisfactory; further analysis is needed. We will repeat our previous measurements and then sacrifice the animal, enucleate the eye to obtain the retina and choroid for in-vitro measurements of reflectivity and transmission. Specular and diffuse reflectivity will be measured in-vivo and in-vitro, and scattered light will be measured in-vivo.

   All of our old data will be reviewed as well as our reference data; and with the new data, we hope to come to a satisfactory understanding of the problem of scattered light in the eye.

7. A monkey who has never had a fluorescein injection will have his retina irradiated with the 488 nm argon ion laser. The retinal fluorescence will be measured as the intensity is varied. We wish to know if the rapid rise to a high value is an indication of retinal damage. If it is, this indicates a change in molecular structure in the retina when a burn is made.

## FIGURE CAPTIONS

Figure 1 Retinal reflectivity values taken during and shortly after a burn was made with a YAG laser.

Figure 2 First data sheet for an argon ion CW laser burn retinal reflectivity experiment.

Figure 3 Retinal reflectivity versus wavelength before and during an argon ion CW laser burn retinal reflectivity experiment.

Figure 4 Retinal reflectivity versus wavelength after an argon ion CW laser burn retinal reflectivity experiment.

Figure 5 Time history of retinal reflectivity for an argon ion CW laser burn retinal reflectivity experiment. Wavelengths 462, 540 nm.

Figure 6 Time history of retinal reflectivity for an argon ion CW laser burn retinal reflectivity experiment. Wavelengths 658, 760 nm.

Figure 7 Time history of retinal reflectivity for an argon ion pulsed laser burn retinal reflectivity experiment. Wavelengths 462, 540, 658, 695 nm.

Figure 8 "Trend" plots of time history of laser burns shown in Figure 7.

Figure 9 Retinal reflectivity data for every fifth wavelength scan for data plotted in Figure 7.

Figure 10 Fluorescence spectra of retina illuminated with 488 nm argon ion laser.

Figure 11 Time history of fluorescent energy at 462, 540, 658 and 695 nm.

Figure 12 Monochromatic light retinal photograph taken at various times after burns were made on the retina with an argon ion laser.

Figure 13 Changes in retinal reflectivity due to an argon ion laser burn.
Scan 1, before burn
Scan 61, at end of burn period, 470 seconds after start of experiment
Scan 196, at 1100 seconds after start of experiment

Figure 14 A. Retinal reflectivity at 3 degrees from illuminated area
B. Retinal reflectivity on illuminated area
A/B Ratio of energy reflected from nonilluminated to illuminated retinal areas. 450-800 nm.
Note: A and B are not corrected for intensity or instrument transmission.

Figure 15 Ratio of energy reflected from nonilluminated to illuminated retinal areas, 700-900 nm. 20 scans averaged.

Figure 16 Identical to Figure 15 except 200 scans averaged.

Maximum time is 2370.4 s
Lambda is 462 nm

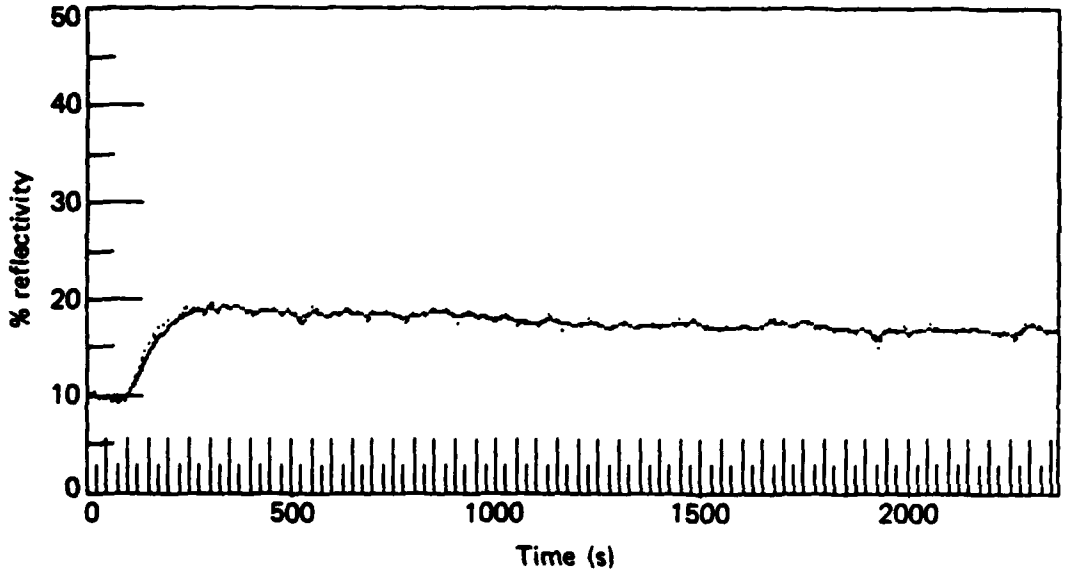


Fig. 1A

Maximum time is 2370.4 s
Lambda is 540 nm

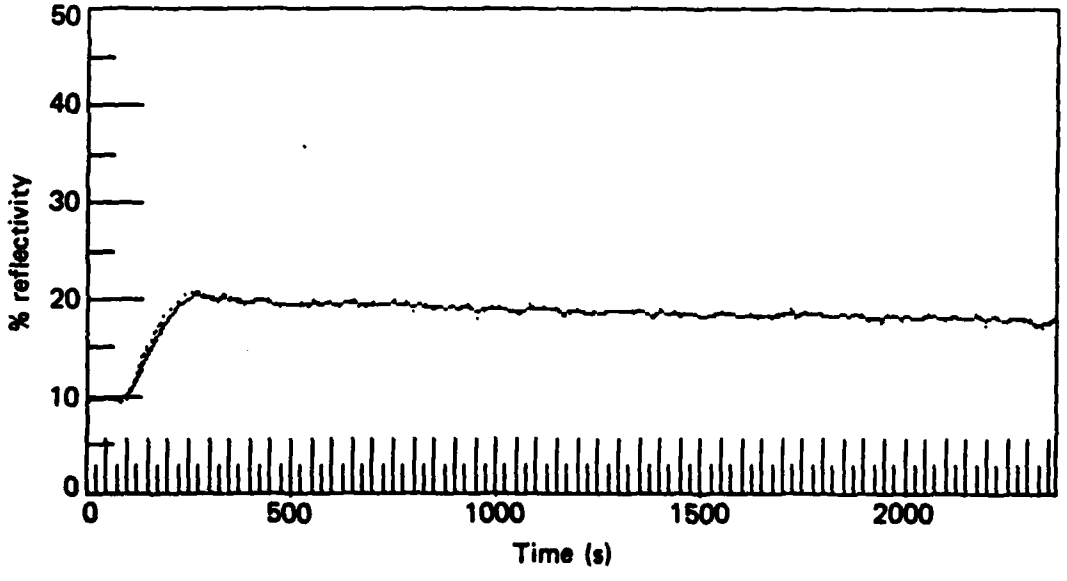


Fig. 1B

Maximum time is 2370.4 s
Lambda is 658 nm

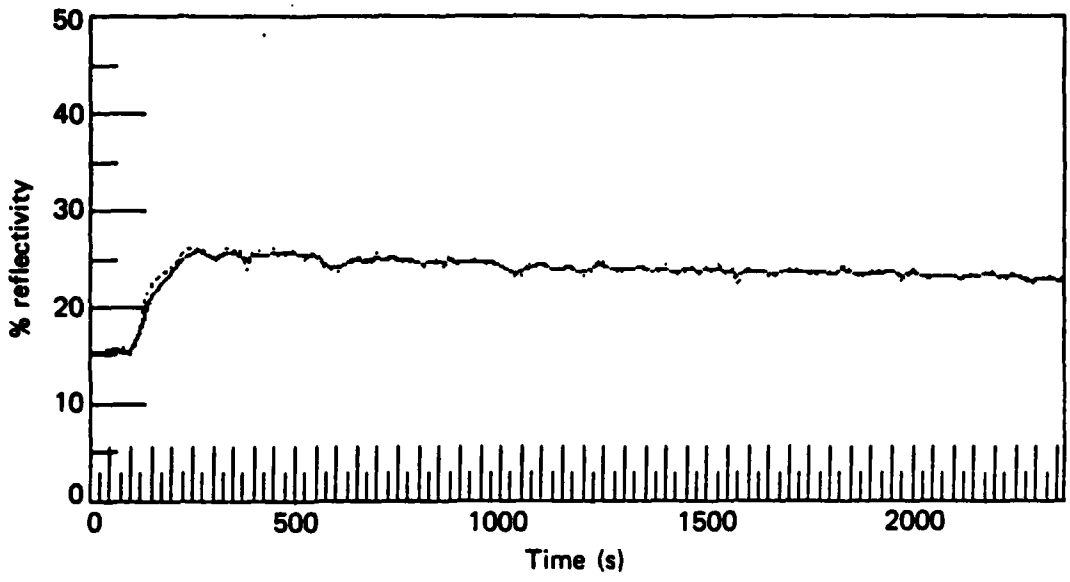


Fig. 1C

Maximum time is 2370.4 s
Lambda is 695 nm

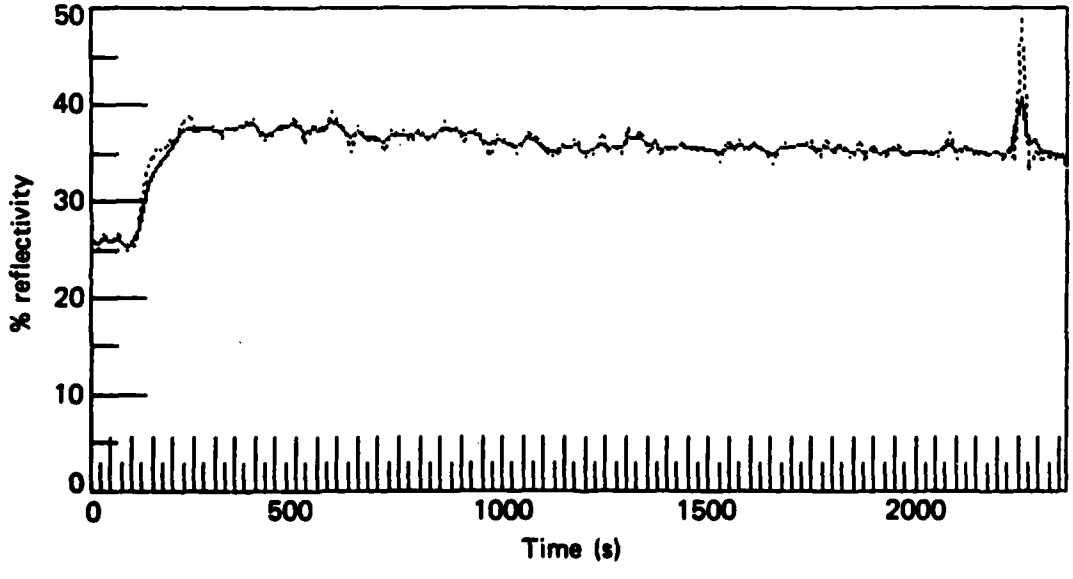


Fig. 1D

Figure 2

DATE IS

THERE WILL BE 200 SCANS

TIME DELAY BETWEEN SCANS IS 0 Sec
RUN TIME WILL BE 17.6666666667 MINUTES
SIGNAL LEVELS FROM STANDARD ARE

| | | | |
|---|---|---|---|
| .04087 | .04372 | .04846 | .05099 |
| .10528 | .93819 | .98578 | .93477 |
| .82208 | .55451 | .05101 | 1.09997 |
| .29215 | .06659 | .04281 | .04667 |
| .04282 | .04061 | .04363 | .04511 |

REFLECTIVITY OF STANDARD IS 10 %
SHUTTER NOT USED

SCAN NO 1 TIME 0 .10021
SCAN NO 2 TIME 5.3 .1017
SCAN NO 3 TIME 10.6 .1099
SCAN NO 4 TIME 15.9 .10667
SCAN NO 5 TIME 21.2 .1129
SCAN NO 6 TIME 26.5 .65783
SCAN NO 7 TIME 31.8 .52885
SCAN NO 8 TIME 37.1 .4833
SCAN NO 9 TIME 42.4 .4598
SCAN NO 10 TIME 47.7 .44918
SCAN NO 11 TIME 53 .4327
SCAN NO 12 TIME 58.3 .39478
SCAN NO 13 TIME 63.6 .39773
SCAN NO 14 TIME 68.9 .3715
SCAN NO 15 TIME 74.2 .37182
SCAN NO 16 TIME 79.5 .37116
SCAN NO 17 TIME 84.8 .37081
SCAN NO 18 TIME 90.1 .35694
SCAN NO 19 TIME 95.4 .34834
SCAN NO 20 TIME 100.7 .33987
SCAN NO 21 TIME 106 .34969
SCAN NO 22 TIME 111.3 .34876
SCAN NO 23 TIME 116.6 .14271
SCAN NO 24 TIME 121.9 .13725
SCAN NO 25 TIME 127.2 .14525
SCAN NO 26 TIME 132.5 .14418
SCAN NO 27 TIME 137.8 .13309
SCAN NO 28 TIME 143.1 .13696
SCAN NO 29 TIME 148.4 .14452
SCAN NO 30 TIME 153.7 .13076
SCAN NO 31 TIME 159 .13456
SCAN NO 32 TIME 164.3 .13338
SCAN NO 33 TIME 169.6 .13284
SCAN NO 34 TIME 174.9 .14611
SCAN NO 35 TIME 180.2 .13361
SCAN NO 36 TIME 185.5 .12981
SCAN NO 37 TIME 190.8 .13981
SCAN NO 38 TIME 196.1 .12932
SCAN NO 39 TIME 201.4 .12896
SCAN NO 40 TIME 206.7 .13145
SCAN NO 41 TIME 212 .13282
SCAN NO 42 TIME 217.3 .13572
SCAN NO 43 TIME 222.6 .1364

Short lambda .571 DIV/nm, long lambda .34 DIV/nm
546.1 nm is at 118 divisions, 200 divisions is 660 nm
Scan time is 0

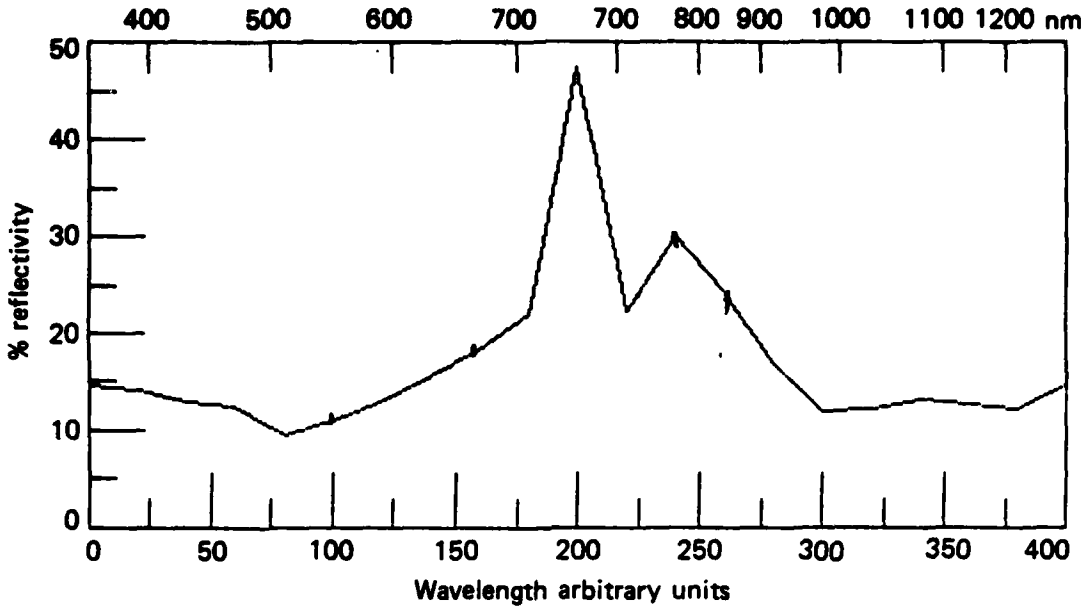


Fig. 3A

Scan time is 106

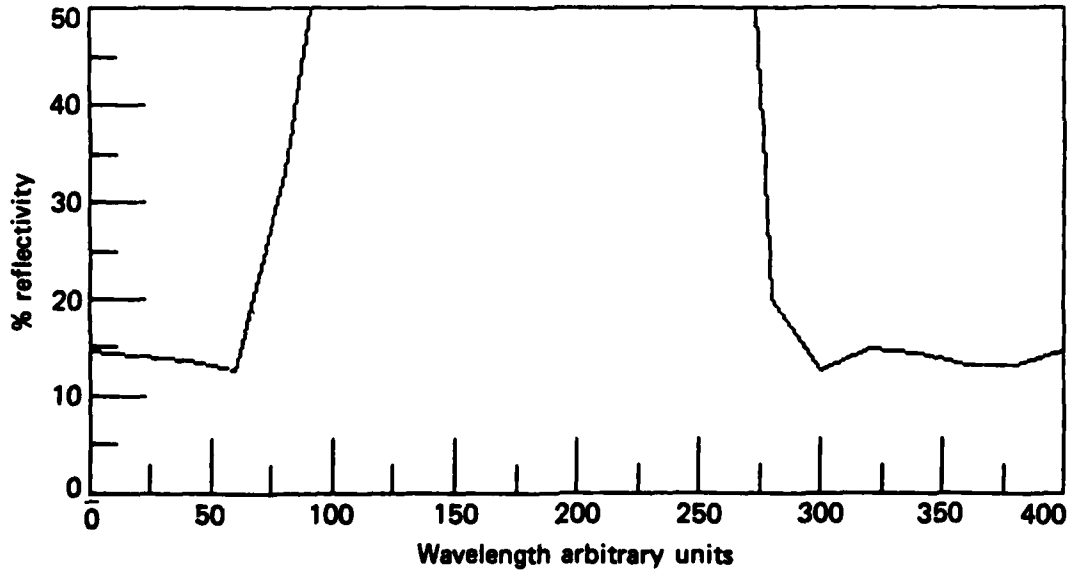


Fig. 3B

Scan time is 424.1

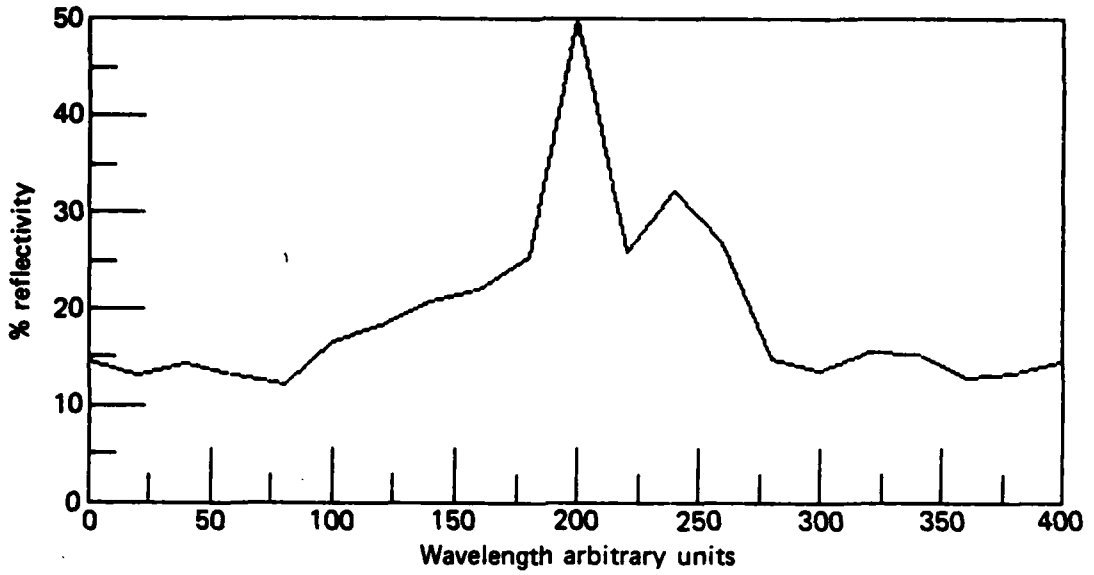


Fig. 4A

Scan time is 530.1

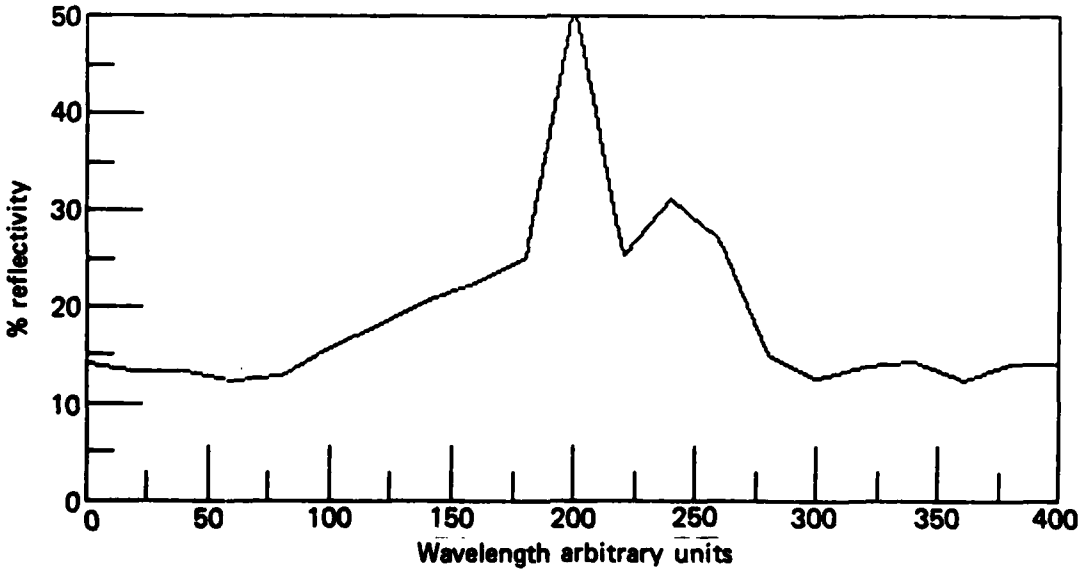


Fig. 4B

Maximum time is 1054.7 s
Lambda is 462 nm

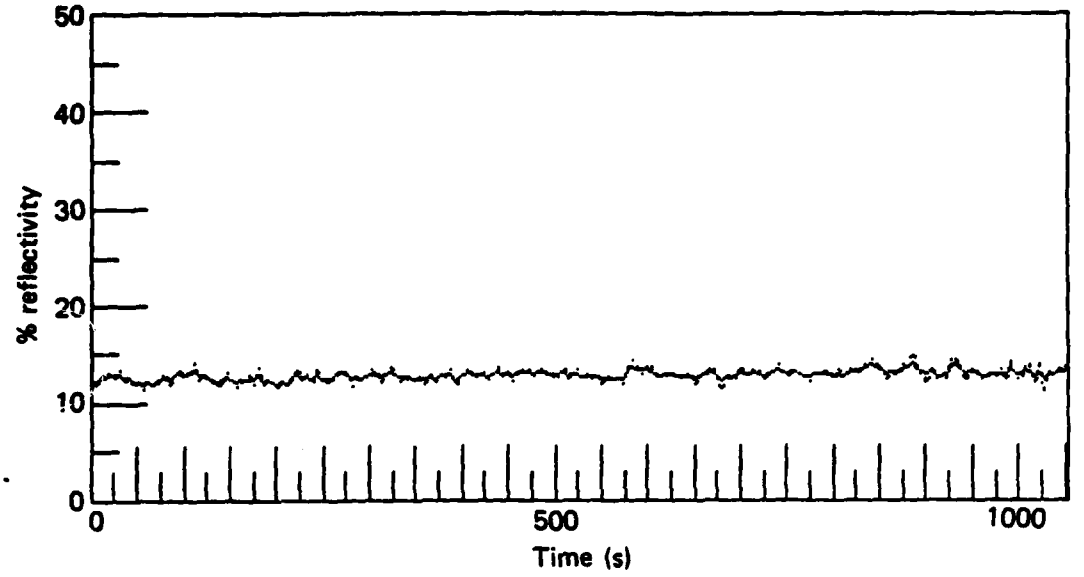


Fig. 5A

Maximum time is 1054.7 s
Lambda is 540 nm

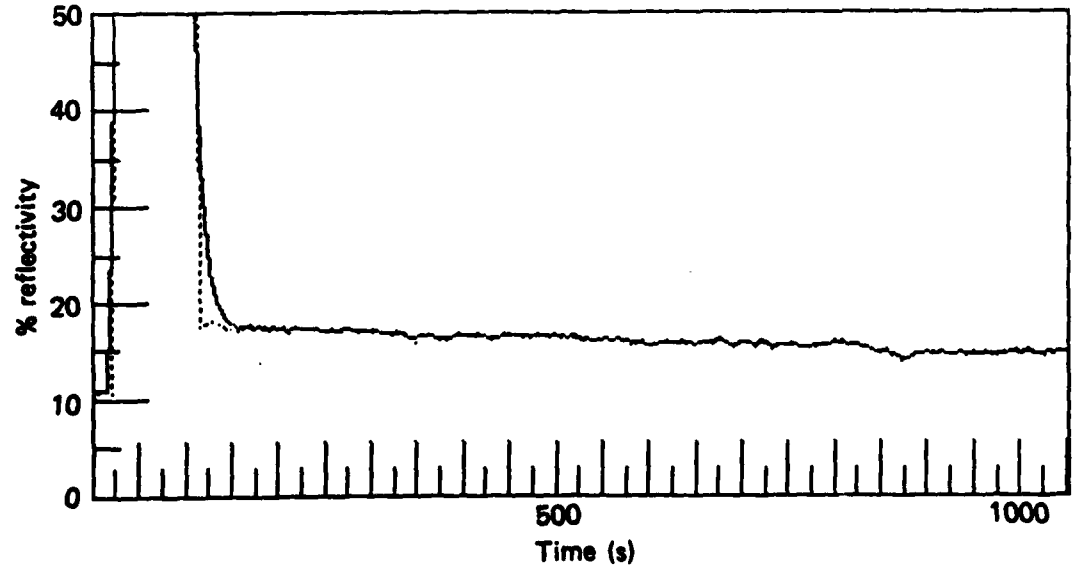


Fig. 5B

Maximum time is 1054.7 s
Lambda is 658 nm

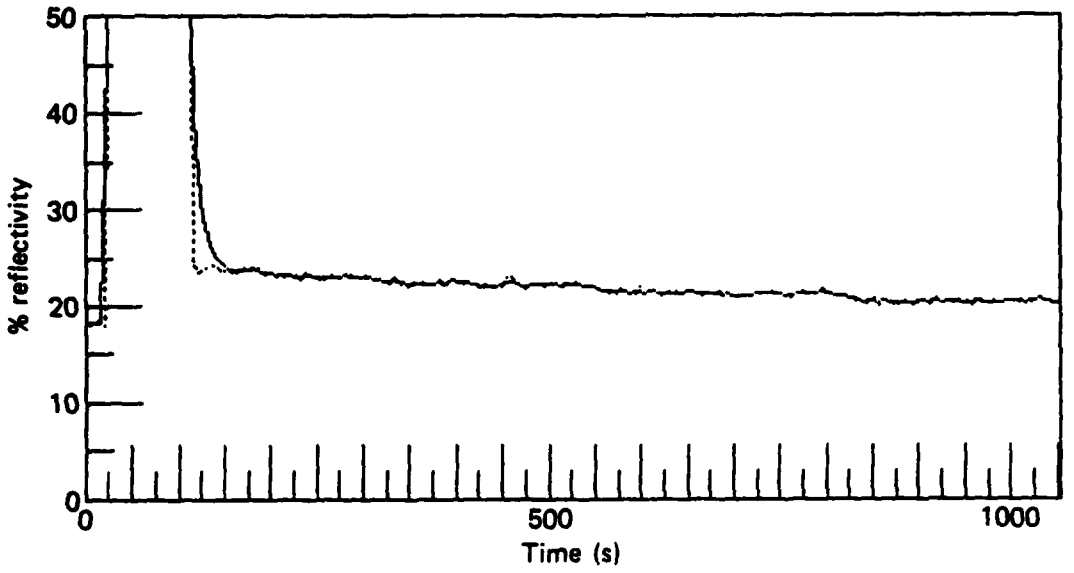


Fig. 6A

Maximum time is 1054.7 s
Lambda is 760 nm

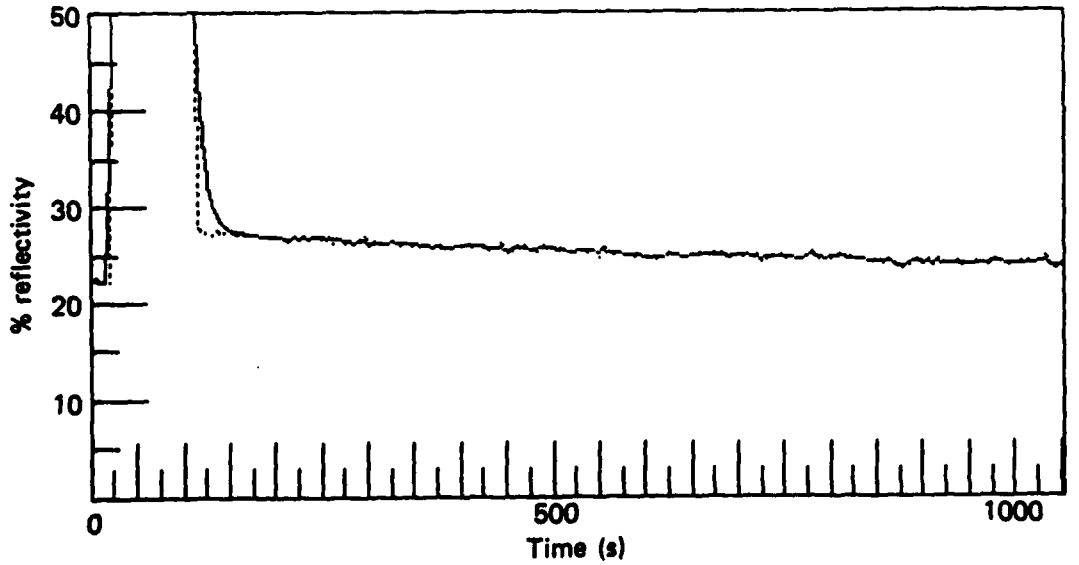


Fig. 6B

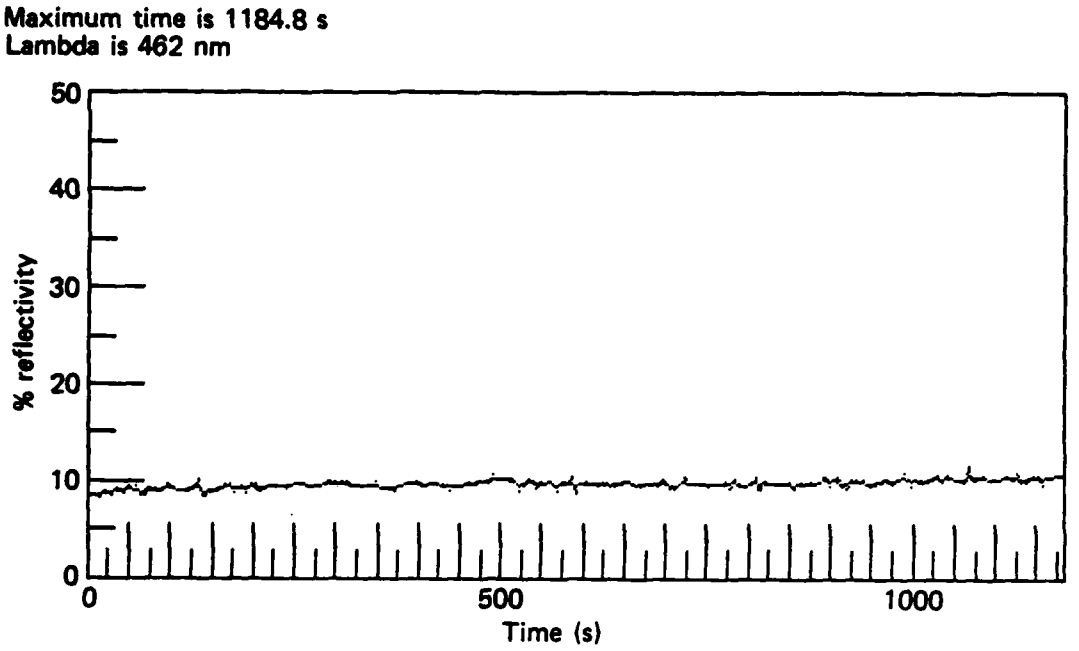
Maximum time is 1184.8 s
Lambda is 462 nm
50
40
30
20
10
0
% reflectivity
0
500
1000
Time (s)

Fig. 7A

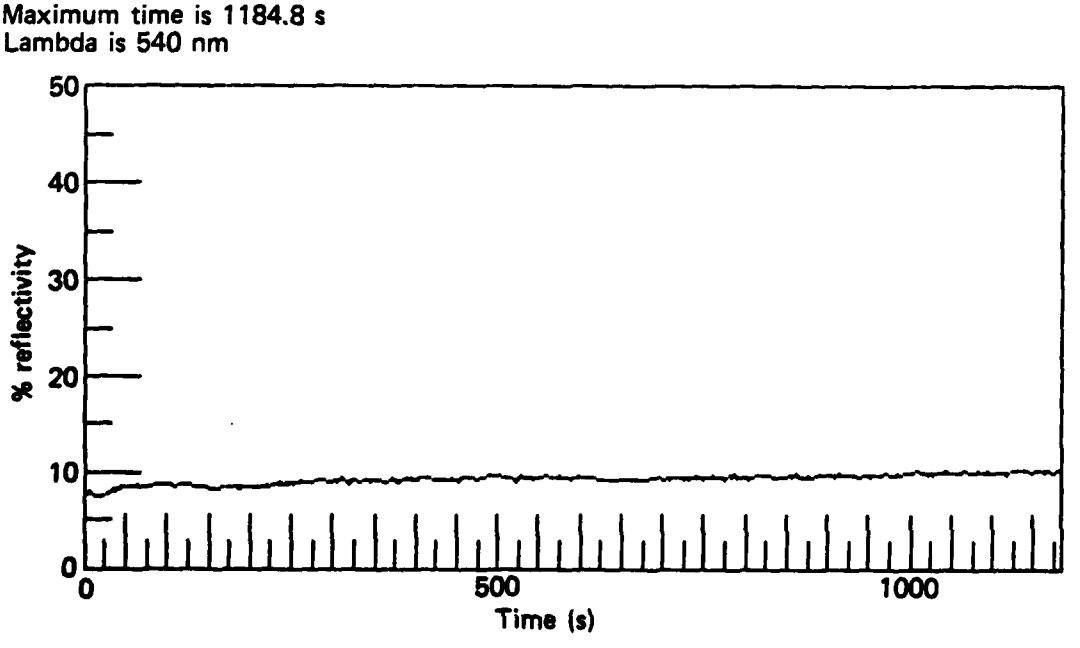
Maximum time is 1184.8 s
Lambda is 540 nm
50
40
30
20
10
0
% reflectivity
0
500
1000
Time (s)

Fig. 7B

Maximum time is 1184.8 s
Lambda is 658 nm

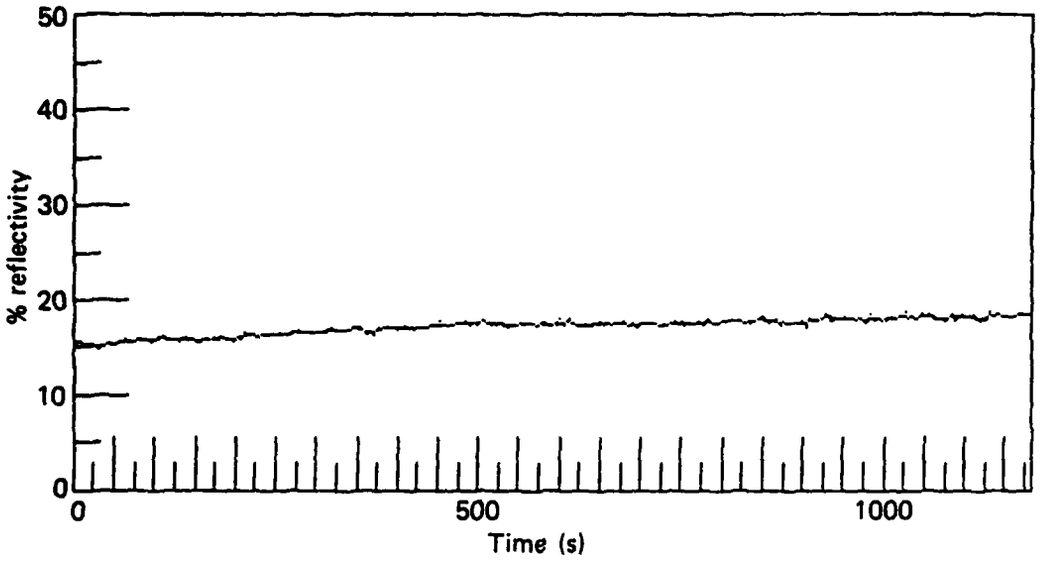


Fig. 7C

Maximum time is 1184.8 s
Lambda is 695 nm

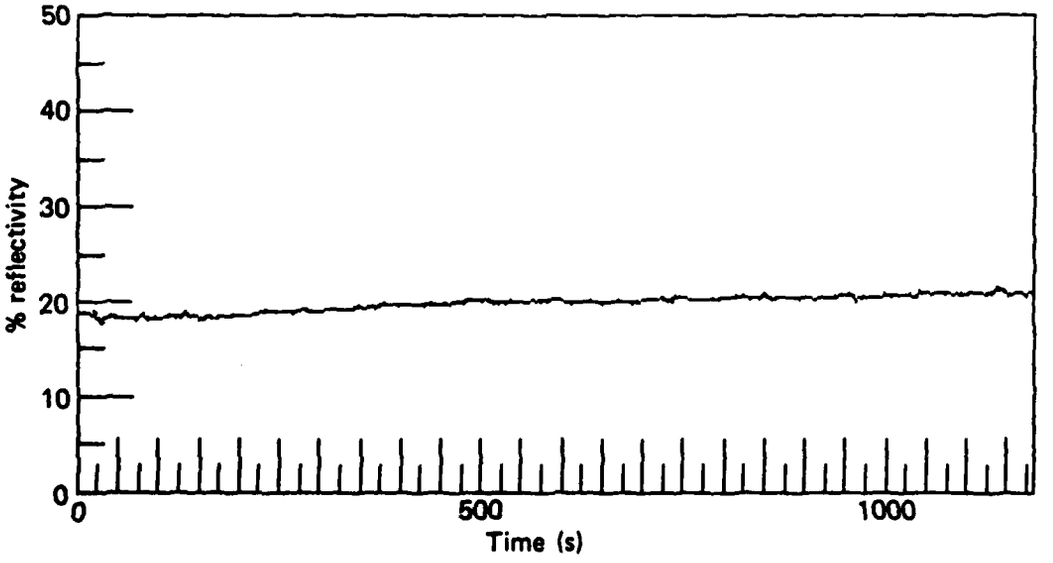


Fig. 7D

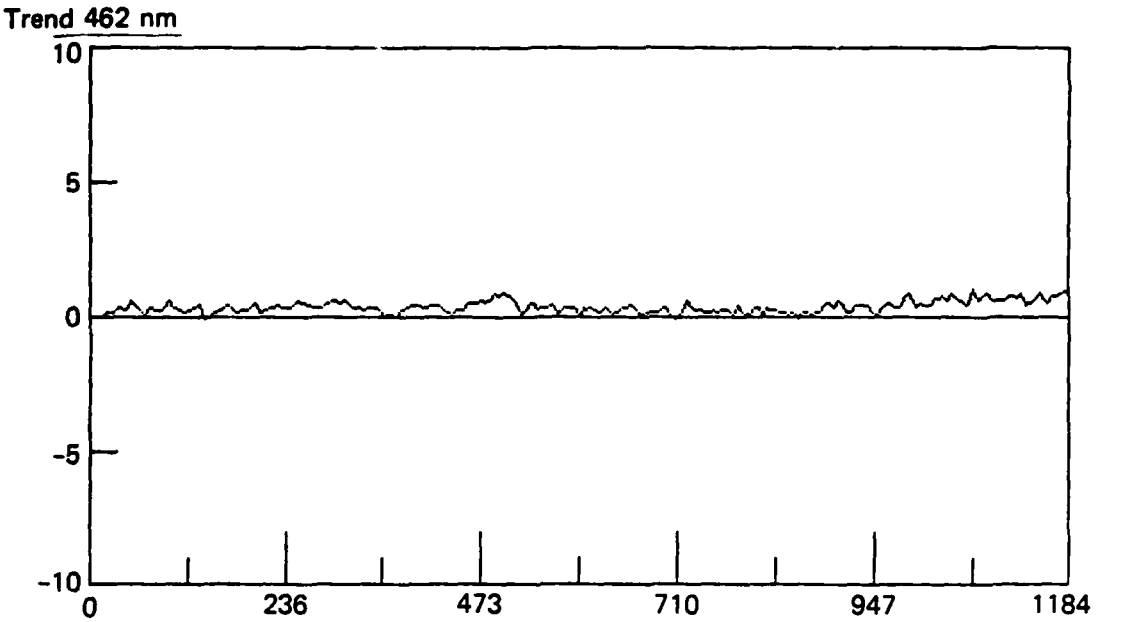
Trend 462 nm
10
5
0
-5
-10
0
236
473
710
947
1184

Fig. 8A

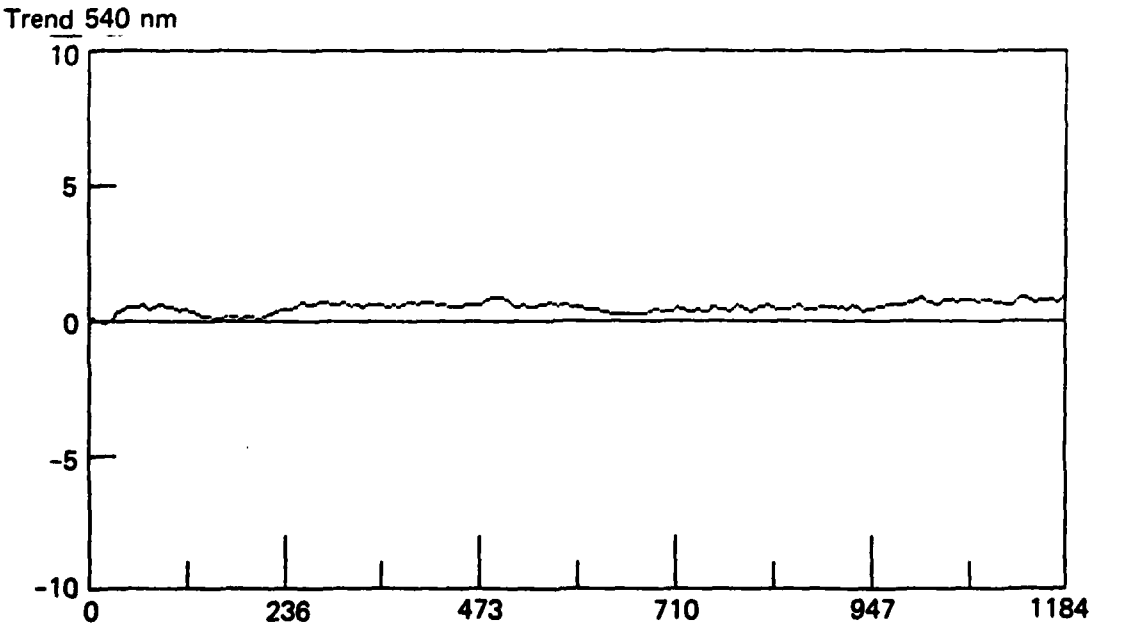
Trend 540 nm
10
5
0
-5
-10
0
236
473
710
947
1184

Fig. 8B

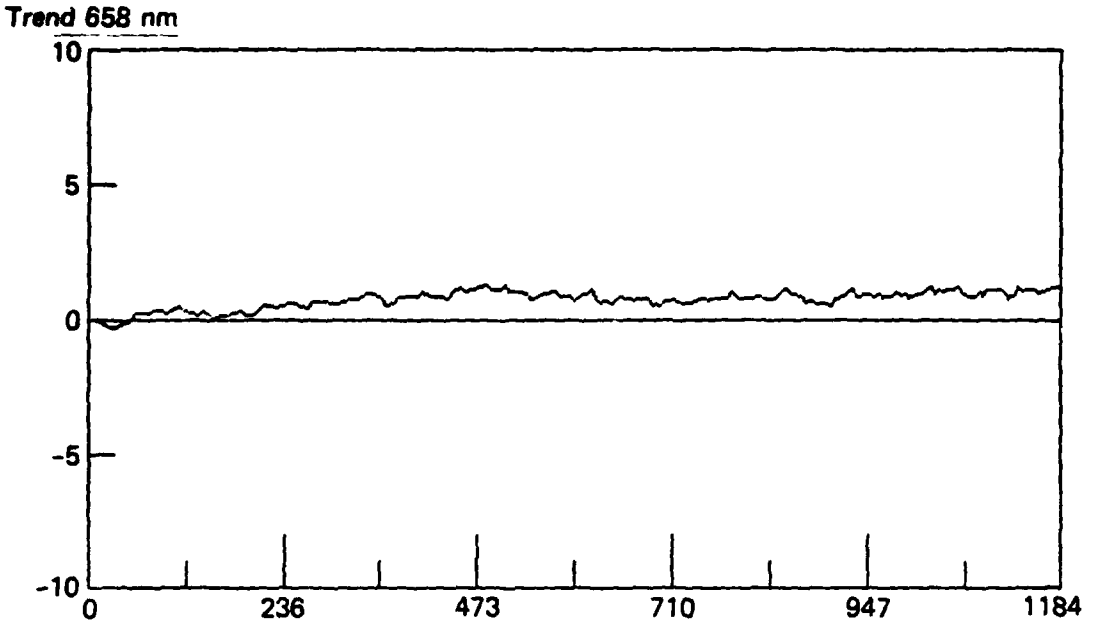
Trend 658 nm
10
5
0
-5
-10
0
236
473
710
947
1184

Fig. 8C

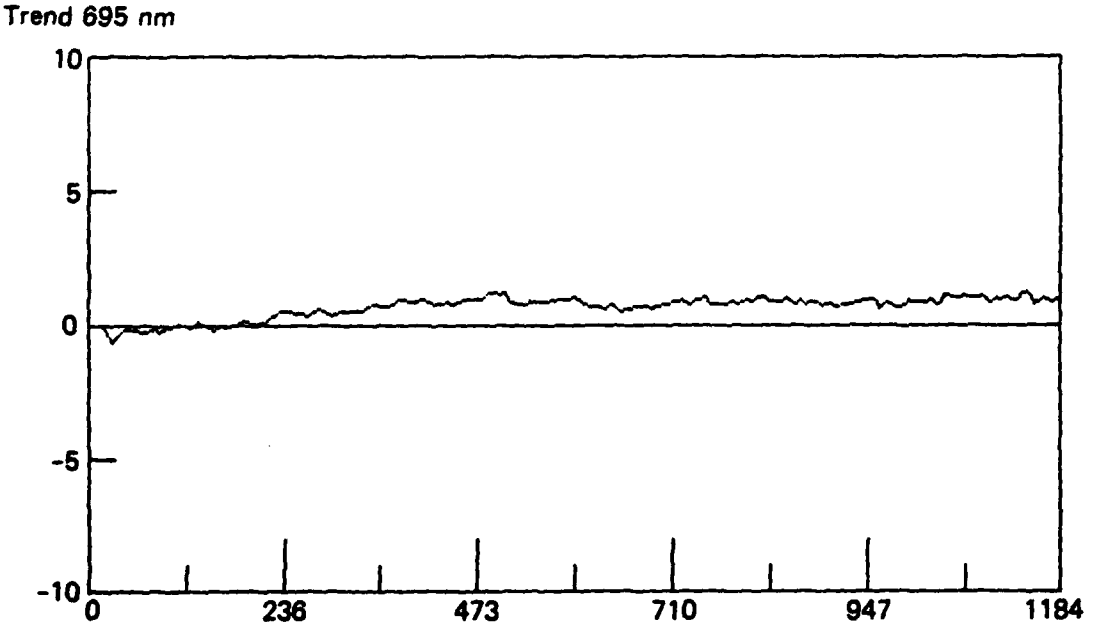
Trend 695 nm
10
5
0
-5
-10
0
236
473
710
947
1184

Fig. 8D

Figure 9A

| | | | | | | |
|---|---|---|---|---|---|---|
| Scan | 1.00E+00 | 1.22E+01 | 1.13E+01 | 1.21E+01 | 8.50E+00 | 8.42E+00 |
| Scan | 6.00E+00 | 1.08E+01 | 1.18E+01 | 1.22E+01 | 8.68E+00 | 8.19E+00 |
| Scan | 1.10E+01 | 1.29E+01 | 1.15E+01 | 1.29E+01 | 8.80E+00 | 8.66E+00 |
| Scan | 1.60E+01 | 1.28E+01 | 1.06E+01 | 1.30E+01 | 9.21E+00 | 8.60E+00 |
| Scan | 2.10E+01 | 1.11E+01 | 1.14E+01 | 1.21E+01 | 8.84E+00 | 8.77E+00 |
| Scan | 2.60E+01 | 1.17E+01 | 1.28E+01 | 1.28E+01 | 9.13E+00 | 8.63E+00 |
| Scan | 3.10E+01 | 1.18E+01 | 1.16E+01 | 1.29E+01 | 9.26E+00 | 8.89E+00 |
| Scan | 3.60E+01 | 1.23E+01 | 1.16E+01 | 1.41E+01 | 9.72E+00 | 9.17E+00 |
| Scan | 4.10E+01 | 1.26E+01 | 1.12E+01 | 1.20E+01 | 9.69E+00 | 9.31E+00 |
| Scan | 4.60E+01 | 1.22E+01 | 1.09E+01 | 1.32E+01 | 9.50E+00 | 9.09E+00 |
| Scan | 5.10E+01 | 1.24E+01 | 1.06E+01 | 1.31E+01 | 9.27E+00 | 9.23E+00 |
| Scan | 5.60E+01 | 1.23E+01 | 1.16E+01 | 1.26E+01 | 9.69E+00 | 9.66E+00 |
| Scan | 6.10E+01 | 1.13E+01 | 1.22E+01 | 1.29E+01 | 9.36E+00 | 9.47E+00 |
| Scan | 6.60E+01 | 1.14E+01 | 1.15E+01 | 1.23E+01 | 9.95E+00 | 9.68E+00 |
| Scan | 7.10E+01 | 1.17E+01 | 1.15E+01 | 1.35E+01 | 1.02E+01 | 9.61E+00 |
| Scan | 7.60E+01 | 1.13E+01 | 1.16E+01 | 1.41E+01 | 9.64E+00 | 9.87E+00 |
| Scan | 8.10E+01 | 1.33E+01 | 1.13E+01 | 1.31E+01 | 9.78E+00 | 9.79E+00 |
| Scan | 8.60E+01 | 1.14E+01 | 1.15E+01 | 1.35E+01 | 9.75E+00 | 9.71E+00 |
| Scan | 9.10E+01 | 1.22E+01 | 1.06E+01 | 1.33E+01 | 9.81E+00 | 9.37E+00 |
| Scan | 9.60E+01 | 1.18E+01 | 1.09E+01 | 1.28E+01 | 9.52E+00 | 9.32E+00 |
| Scan | 1.01E+02 | 1.15E+01 | 1.29E+01 | 1.19E+01 | 9.75E+00 | 9.03E+00 |
| Scan | 1.06E+02 | 1.13E+01 | 1.25E+01 | 1.21E+01 | 9.64E+00 | 9.59E+00 |
| Scan | 1.11E+02 | 1.20E+01 | 1.12E+01 | 1.39E+01 | 9.58E+00 | 9.70E+00 |
| Scan | 1.16E+02 | 1.10E+01 | 1.15E+01 | 1.30E+01 | 9.79E+00 | 9.75E+00 |
| Scan | 1.21E+02 | 1.14E+01 | 1.05E+01 | 1.34E+01 | 9.80E+00 | 9.82E+00 |
| Scan | 1.26E+02 | 1.31E+01 | 1.24E+01 | 1.30E+01 | 9.58E+00 | 9.83E+00 |
| Scan | 1.31E+02 | 1.14E+01 | 1.14E+01 | 1.32E+01 | 9.84E+00 | 9.88E+00 |
| Scan | 1.36E+02 | 1.10E+01 | 1.17E+01 | 1.32E+01 | 9.66E+00 | 9.78E+00 |
| Scan | 1.41E+02 | 1.30E+01 | 1.14E+01 | 1.29E+01 | 9.60E+00 | 9.64E+00 |
| Scan | 1.46E+02 | 1.21E+01 | 1.20E+01 | 1.39E+01 | 9.87E+00 | 9.94E+00 |
| Scan | 1.51E+02 | 1.20E+01 | 1.20E+01 | 1.31E+01 | 9.97E+00 | 9.67E+00 |
| Scan | 1.56E+02 | 1.24E+01 | 1.11E+01 | 1.46E+01 | 9.70E+00 | 1.01E+01 |
| Scan | 1.61E+02 | 1.20E+01 | 1.11E+01 | 1.28E+01 | 9.94E+00 | 9.96E+00 |
| Scan | 1.66E+02 | 1.31E+01 | 1.20E+01 | 1.33E+01 | 1.01E+01 | 9.93E+00 |
| Scan | 1.71E+02 | 1.31E+01 | 1.22E+01 | 1.34E+01 | 1.04E+01 | 1.01E+01 |
| Scan | 1.76E+02 | 1.10E+01 | 1.19E+01 | 1.37E+01 | 1.01E+01 | 9.77E+00 |
| Scan | 1.81E+02 | 1.23E+01 | 1.33E+01 | 1.29E+01 | 1.06E+01 | 1.04E+01 |
| Scan | 1.86E+02 | 1.30E+01 | 1.14E+01 | 1.29E+01 | 1.05E+01 | 1.03E+01 |
| Scan | 1.91E+02 | 1.19E+01 | 1.10E+01 | 1.46E+01 | 1.02E+01 | 1.00E+01 |
| Scan | 1.96E+02 | 1.31E+01 | 1.15E+01 | 1.26E+01 | 1.05E+01 | 1.01E+01 |

| | | | | | | |
|---|---|---|---|---|---|---|
| Scan | 1.00E+00 | 7.62E+00 | 8.69E+00 | 1.24E+01 | 1.56E+01 | 1.92E+01 |
| Scan | 6.00E+00 | 7.75E+00 | 8.95E+00 | 1.17E+01 | 1.50E+01 | 1.76E+01 |
| Scan | 1.10E+01 | 8.55E+00 | 1.00E+01 | 1.30E+01 | 1.56E+01 | 1.87E+01 |
| Scan | 1.60E+01 | 8.66E+00 | 9.92E+00 | 1.35E+01 | 1.59E+01 | 1.84E+01 |
| Scan | 2.10E+01 | 8.47E+00 | 9.87E+00 | 1.27E+01 | 1.59E+01 | 1.87E+01 |
| Scan | 2.60E+01 | 8.48E+00 | 9.63E+00 | 1.35E+01 | 1.59E+01 | 1.89E+01 |
| Scan | 3.10E+01 | 8.51E+00 | 9.66E+00 | 1.33E+01 | 1.63E+01 | 1.88E+01 |
| Scan | 3.60E+01 | 8.91E+00 | 1.01E+01 | 1.35E+01 | 1.64E+01 | 1.90E+01 |
| Scan | 4.10E+01 | 9.14E+00 | 1.04E+01 | 1.38E+01 | 1.65E+01 | 1.91E+01 |
| Scan | 4.60E+01 | 9.13E+00 | 1.06E+01 | 1.40E+01 | 1.67E+01 | 1.97E+01 |
| Scan | 5.10E+01 | 9.10E+00 | 1.05E+01 | 1.45E+01 | 1.66E+01 | 1.99E+01 |
| Scan | 5.60E+01 | 9.30E+00 | 1.07E+01 | 1.41E+01 | 1.70E+01 | 1.98E+01 |
| Scan | 6.10E+01 | 9.27E+00 | 1.09E+01 | 1.41E+01 | 1.70E+01 | 1.99E+01 |
| Scan | 6.60E+01 | 9.34E+00 | 1.11E+01 | 1.45E+01 | 1.75E+01 | 2.06E+01 |
| Scan | 7.10E+01 | 9.67E+00 | 1.12E+01 | 1.47E+01 | 1.75E+01 | 2.06E+01 |
| Scan | 7.60E+01 | 9.50E+00 | 1.08E+01 | 1.44E+01 | 1.75E+01 | 2.03E+01 |
| Scan | 8.10E+01 | 9.53E+00 | 1.09E+01 | 1.47E+01 | 1.75E+01 | 2.00E+01 |
| Scan | 8.60E+01 | 9.54E+00 | 1.07E+01 | 1.48E+01 | 1.75E+01 | 2.04E+01 |

Figure 9B

| | | | | | | |
|---|---|---|---|---|---|---|
| Scan | 9.10E+01 | 9.42E+00 | 1.08E+01 | 1.45E+01 | 1.76E+01 | 1.97E+01 |
| Scan | 9.60E+01 | 9.25E+00 | 1.07E+01 | 1.44E+01 | 1.73E+01 | 2.05E+01 |
| Scan | 1.01E+02 | 9.25E+00 | 1.08E+01 | 1.43E+01 | 1.75E+01 | 2.00E+01 |
| Scan | 1.06E+02 | 9.43E+00 | 1.12E+01 | 1.49E+01 | 1.73E+01 | 2.01E+01 |
| Scan | 1.11E+02 | 9.51E+00 | 1.08E+01 | 1.48E+01 | 1.75E+01 | 2.03E+01 |
| Scan | 1.16E+02 | 9.49E+00 | 1.08E+01 | 1.45E+01 | 1.75E+01 | 2.07E+01 |
| Scan | 1.21E+02 | 9.49E+00 | 1.09E+01 | 1.46E+01 | 1.76E+01 | 1.98E+01 |
| Scan | 1.26E+02 | 9.57E+00 | 1.08E+01 | 1.49E+01 | 1.76E+01 | 2.07E+01 |
| Scan | 1.31E+02 | 9.65E+00 | 1.09E+01 | 1.49E+01 | 1.78E+01 | 2.06E+01 |
| Scan | 1.36E+02 | 9.53E+00 | 1.10E+01 | 1.49E+01 | 1.80E+01 | 2.11E+01 |
| Scan | 1.41E+02 | 9.53E+00 | 1.13E+01 | 1.48E+01 | 1.76E+01 | 2.13E+01 |
| Scan | 1.46E+02 | 9.66E+00 | 1.12E+01 | 1.48E+01 | 1.75E+01 | 2.06E+01 |
| Scan | 1.51E+02 | 9.74E+00 | 1.12E+01 | 1.47E+01 | 1.80E+01 | 2.12E+01 |
| Scan | 1.56E+02 | 9.62E+00 | 1.10E+01 | 1.49E+01 | 1.80E+01 | 2.07E+01 |
| Scan | 1.61E+02 | 9.77E+00 | 1.11E+01 | 1.49E+01 | 1.79E+01 | 2.11E+01 |
| Scan | 1.66E+02 | 1.00E+01 | 1.12E+01 | 1.48E+01 | 1.79E+01 | 2.12E+01 |
| Scan | 1.71E+02 | 9.87E+00 | 1.17E+01 | 1.49E+01 | 1.81E+01 | 2.10E+01 |
| Scan | 1.76E+02 | 1.00E+01 | 1.13E+01 | 1.52E+01 | 1.84E+01 | 2.10E+01 |
| Scan | 1.81E+02 | 1.00E+01 | 1.12E+01 | 1.55E+01 | 1.83E+01 | 2.13E+01 |
| Scan | 1.86E+02 | 9.96E+00 | 1.16E+01 | 1.50E+01 | 1.84E+01 | 2.11E+01 |
| Scan | 1.91E+02 | 1.02E+01 | 1.16E+01 | 1.51E+01 | 1.83E+01 | 2.11E+01 |
| Scan | 1.96E+02 | 1.01E+01 | 1.15E+01 | 1.51E+01 | 1.83E+01 | 2.12E+01 |

| | | | | | | |
|---|---|---|---|---|---|---|
| Scan | 1.00E+00 | 3.75E+01 | 1.89E+01 | 2.89E+01 | 2.71E+01 | 1.10E+01 |
| Scan | 6.00E+00 | 3.65E+01 | 1.80E+01 | 2.66E+01 | 2.64E+01 | 1.26E+01 |
| Scan | 1.10E+01 | 3.49E+01 | 1.83E+01 | 2.77E+01 | 2.53E+01 | 1.24E+01 |
| Scan | 1.60E+01 | 3.64E+01 | 1.84E+01 | 2.68E+01 | 2.57E+01 | 1.19E+01 |
| Scan | 2.10E+01 | 3.72E+01 | 1.85E+01 | 2.73E+01 | 2.54E+01 | 1.21E+01 |
| Scan | 2.60E+01 | 3.59E+01 | 1.84E+01 | 2.69E+01 | 2.57E+01 | 1.28E+01 |
| Scan | 3.10E+01 | 3.84E+01 | 1.86E+01 | 2.67E+01 | 2.54E+01 | 1.39E+01 |
| Scan | 3.60E+01 | 3.84E+01 | 1.90E+01 | 2.65E+01 | 2.58E+01 | 1.26E+01 |
| Scan | 4.10E+01 | 4.02E+01 | 1.91E+01 | 2.66E+01 | 2.54E+01 | 1.20E+01 |
| Scan | 4.60E+01 | 3.55E+01 | 1.92E+01 | 2.72E+01 | 2.57E+01 | 1.27E+01 |
| Scan | 5.10E+01 | 3.64E+01 | 1.94E+01 | 2.65E+01 | 2.50E+01 | 1.29E+01 |
| Scan | 5.60E+01 | 3.59E+01 | 1.97E+01 | 2.79E+01 | 2.53E+01 | 1.28E+01 |
| Scan | 6.10E+01 | 3.95E+01 | 1.97E+01 | 2.83E+01 | 2.58E+01 | 1.40E+01 |
| Scan | 6.60E+01 | 3.84E+01 | 1.99E+01 | 2.79E+01 | 2.52E+01 | 1.26E+01 |
| Scan | 7.10E+01 | 3.75E+01 | 2.02E+01 | 2.81E+01 | 2.62E+01 | 1.14E+01 |
| Scan | 7.60E+01 | 3.73E+01 | 1.99E+01 | 2.67E+01 | 2.57E+01 | 1.24E+01 |
| Scan | 8.10E+01 | 3.80E+01 | 2.00E+01 | 2.76E+01 | 2.58E+01 | 1.28E+01 |
| Scan | 8.60E+01 | 3.68E+01 | 2.01E+01 | 2.84E+01 | 2.53E+01 | 1.24E+01 |
| Scan | 9.10E+01 | 3.89E+01 | 2.00E+01 | 2.81E+01 | 2.55E+01 | 1.18E+01 |
| Scan | 9.60E+01 | 3.75E+01 | 2.00E+01 | 2.68E+01 | 2.61E+01 | 1.11E+01 |
| Scan | 1.01E+02 | 3.90E+01 | 2.00E+01 | 2.81E+01 | 2.62E+01 | 1.18E+01 |
| Scan | 1.06E+02 | 3.84E+01 | 2.00E+01 | 2.83E+01 | 2.59E+01 | 1.24E+01 |
| Scan | 1.11E+02 | 4.21E+01 | 2.02E+01 | 2.78E+01 | 2.52E+01 | 1.21E+01 |
| Scan | 1.16E+02 | 3.88E+01 | 2.04E+01 | 2.96E+01 | 2.60E+01 | 1.22E+01 |
| Scan | 1.21E+02 | 4.09E+01 | 2.03E+01 | 2.76E+01 | 2.52E+01 | 1.26E+01 |
| Scan | 1.26E+02 | 3.91E+01 | 2.03E+01 | 2.77E+01 | 2.59E+01 | 1.23E+01 |
| Scan | 1.31E+02 | 3.82E+01 | 2.06E+01 | 2.84E+01 | 2.66E+01 | 1.22E+01 |
| Scan | 1.36E+02 | 4.04E+01 | 2.04E+01 | 2.78E+01 | 2.56E+01 | 1.27E+01 |
| Scan | 1.41E+02 | 3.83E+01 | 2.04E+01 | 2.84E+01 | 2.52E+01 | 1.23E+01 |
| Scan | 1.46E+02 | 3.89E+01 | 2.05E+01 | 2.80E+01 | 2.59E+01 | 1.37E+01 |
| Scan | 1.51E+02 | 4.04E+01 | 2.04E+01 | 2.88E+01 | 2.61E+01 | 1.29E+01 |
| Scan | 1.56E+02 | 3.92E+01 | 2.07E+01 | 2.89E+01 | 2.64E+01 | 1.20E+01 |
| Scan | 1.61E+02 | 4.00E+01 | 2.05E+01 | 2.83E+01 | 2.65E+01 | 1.28E+01 |
| Scan | 1.66E+02 | 3.77E+01 | 2.06E+01 | 2.67E+01 | 2.58E+01 | 1.27E+01 |
| Scan | 1.71E+02 | 3.76E+01 | 2.06E+01 | 2.88E+01 | 2.62E+01 | 1.28E+01 |
| Scan | 1.76E+02 | 3.77E+01 | 2.08E+01 | 2.84E+01 | 2.65E+01 | 1.20E+01 |
| Scan | 1.81E+02 | 3.79E+01 | 2.08E+01 | 2.78E+01 | 2.62E+01 | 1.27E+01 |
| Scan | 1.86E+02 | 3.95E+01 | 2.09E+01 | 2.91E+01 | 2.63E+01 | 1.27E+01 |
| Scan | 1.91E+02 | 3.85E+01 | 2.12E+01 | 2.92E+01 | 2.61E+01 | 1.21E+01 |
| Scan | 1.96E+02 | 4.03E+01 | 2.10E+01 | 2.89E+01 | 2.66E+01 | 1.18E+01 |

Figure 9C

| | | | | | |
|---|---|---|---|---|---|
| Scan 1.00E+00 | 1.27E+01 | 1.57E+01 | 1.19E+01 | 1.04E+01 | 1.19E+01 |
| Scan 6.00E+00 | 1.25E+01 | 1.32E+01 | 1.40E+01 | 1.18E+01 | 1.15E+01 |
| Scan 1.10E+01 | 1.30E+01 | 1.31E+01 | 1.34E+01 | 1.10E+01 | 1.13E+01 |
| Scan 1.60E+01 | 1.20E+01 | 1.33E+01 | 1.29E+01 | 1.27E+01 | 1.09E+01 |
| Scan 2.10E+01 | 1.27E+01 | 1.24E+01 | 1.17E+01 | 1.07E+01 | 1.20E+01 |
| Scan 2.60E+01 | 1.27E+01 | 1.40E+01 | 1.45E+01 | 1.16E+01 | 1.10E+01 |
| Scan 3.10E+01 | 1.41E+01 | 1.51E+01 | 1.30E+01 | 1.15E+01 | 1.30E+01 |
| Scan 3.60E+01 | 1.27E+01 | 1.30E+01 | 1.36E+01 | 1.17E+01 | 1.29E+01 |
| Scan 4.10E+01 | 1.27E+01 | 1.36E+01 | 1.33E+01 | 1.10E+01 | 1.32E+01 |
| Scan 4.60E+01 | 1.25E+01 | 1.43E+01 | 1.35E+01 | 1.12E+01 | 1.11E+01 |
| Scan 5.10E+01 | 1.29E+01 | 1.26E+01 | 1.39E+01 | 1.21E+01 | 1.16E+01 |
| Scan 5.60E+01 | 1.33E+01 | 1.40E+01 | 1.35E+01 | 1.15E+01 | 1.18E+01 |
| Scan 6.10E+01 | 1.29E+01 | 1.42E+01 | 1.31E+01 | 1.11E+01 | 1.33E+01 |
| Scan 6.60E+01 | 1.29E+01 | 1.40E+01 | 1.49E+01 | 1.09E+01 | 1.26E+01 |
| Scan 7.10E+01 | 1.26E+01 | 1.49E+01 | 1.32E+01 | 1.15E+01 | 1.20E+01 |
| Scan 7.60E+01 | 1.26E+01 | 1.24E+01 | 1.47E+01 | 1.15E+01 | 1.31E+01 |
| Scan 8.10E+01 | 1.34E+01 | 1.43E+01 | 1.33E+01 | 1.13E+01 | 1.29E+01 |
| Scan 8.60E+01 | 1.29E+01 | 1.29E+01 | 1.20E+01 | 1.10E+01 | 1.21E+01 |
| Scan 9.10E+01 | 1.28E+01 | 1.38E+01 | 1.34E+01 | 1.15E+01 | 1.17E+01 |
| Scan 9.60E+01 | 1.29E+01 | 1.55E+01 | 1.32E+01 | 1.30E+01 | 1.25E+01 |
| Scan 1.01E+02 | 1.28E+01 | 1.46E+01 | 1.35E+01 | 1.10E+01 | 1.17E+01 |
| Scan 1.06E+02 | 1.32E+01 | 1.44E+01 | 1.28E+01 | 1.14E+01 | 1.26E+01 |
| Scan 1.11E+02 | 1.24E+01 | 1.27E+01 | 1.54E+01 | 1.11E+01 | 1.29E+01 |
| Scan 1.16E+02 | 1.32E+01 | 1.33E+01 | 1.28E+01 | 1.22E+01 | 1.23E+01 |
| Scan 1.21E+02 | 1.31E+01 | 1.28E+01 | 1.40E+01 | 1.13E+01 | 1.27E+01 |
| Scan 1.26E+02 | 1.26E+01 | 1.38E+01 | 1.38E+01 | 1.18E+01 | 1.32E+01 |
| Scan 1.31E+02 | 1.33E+01 | 1.42E+01 | 1.39E+01 | 1.18E+01 | 1.05E+01 |
| Scan 1.36E+02 | 1.30E+01 | 1.42E+01 | 1.31E+01 | 1.11E+01 | 1.22E+01 |
| Scan 1.41E+02 | 1.23E+01 | 1.44E+01 | 1.39E+01 | 1.17E+01 | 1.14E+01 |
| Scan 1.46E+02 | 1.29E+01 | 1.39E+01 | 1.31E+01 | 1.09E+01 | 1.14E+01 |
| Scan 1.51E+02 | 1.34E+01 | 1.42E+01 | 1.34E+01 | 1.15E+01 | 1.26E+01 |
| Scan 1.56E+02 | 1.25E+01 | 1.44E+01 | 1.32E+01 | 1.04E+01 | 1.18E+01 |
| Scan 1.61E+02 | 1.31E+01 | 1.45E+01 | 1.23E+01 | 1.08E+01 | 1.24E+01 |
| Scan 1.66E+02 | 1.31E+01 | 1.37E+01 | 1.36E+01 | 1.15E+01 | 1.21E+01 |
| Scan 1.71E+02 | 1.33E+01 | 1.39E+01 | 1.36E+01 | 1.14E+01 | 1.15E+01 |
| Scan 1.76E+02 | 1.34E+01 | 1.45E+01 | 1.40E+01 | 1.26E+01 | 1.31E+01 |
| Scan 1.81E+02 | 1.29E+01 | 1.28E+01 | 1.38E+01 | 1.27E+01 | 1.23E+01 |
| Scan 1.86E+02 | 1.38E+01 | 1.48E+01 | 1.43E+01 | 1.05E+01 | 1.24E+01 |
| Scan 1.91E+02 | 1.28E+01 | 1.49E+01 | 1.36E+01 | 1.21E+01 | 1.31E+01 |
| Scan 1.96E+02 | 1.30E+01 | 1.35E+01 | 1.37E+01 | 1.14E+01 | 1.17E+01 |

NO MULTIPROGRAMMER ERRORS
FINISHED

Scan time is 106

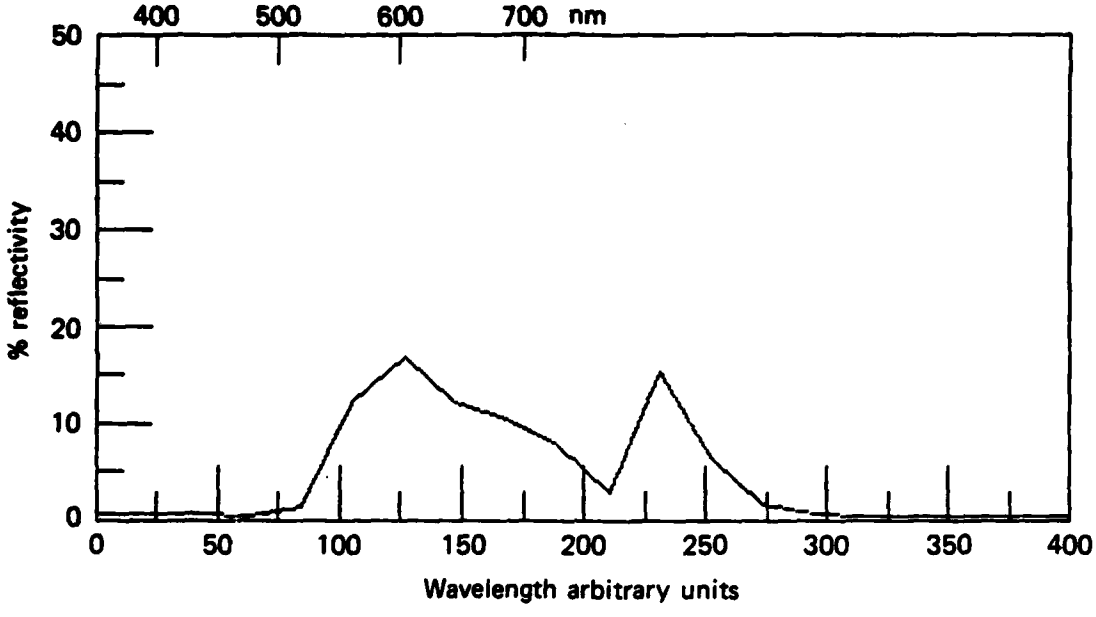


Fig. 10

Maximum time is 127.2 s
Lambda is 462 nm

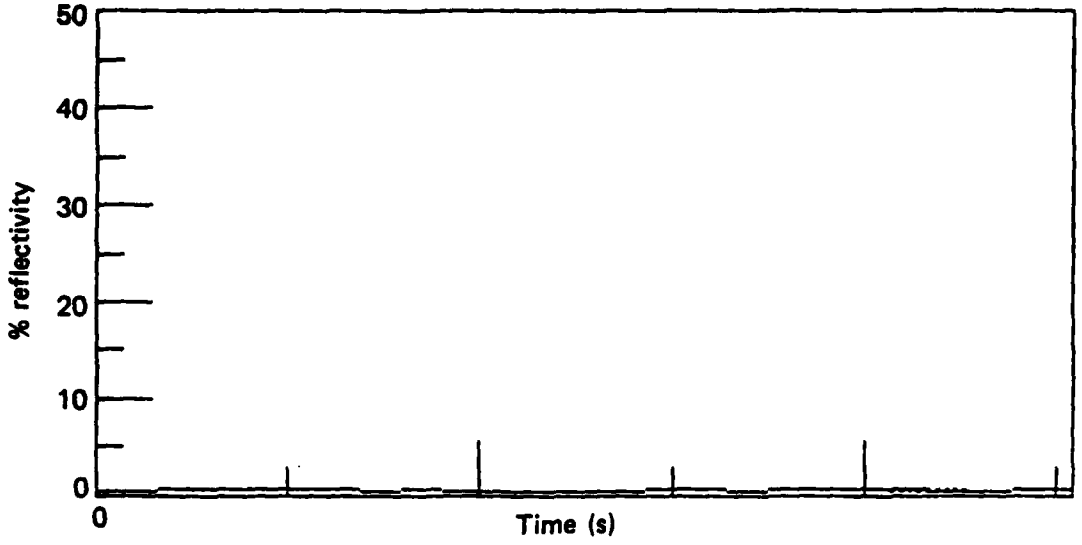


Fig. 11A

Maximum time is 127.2 s
Lambda is 540 nm

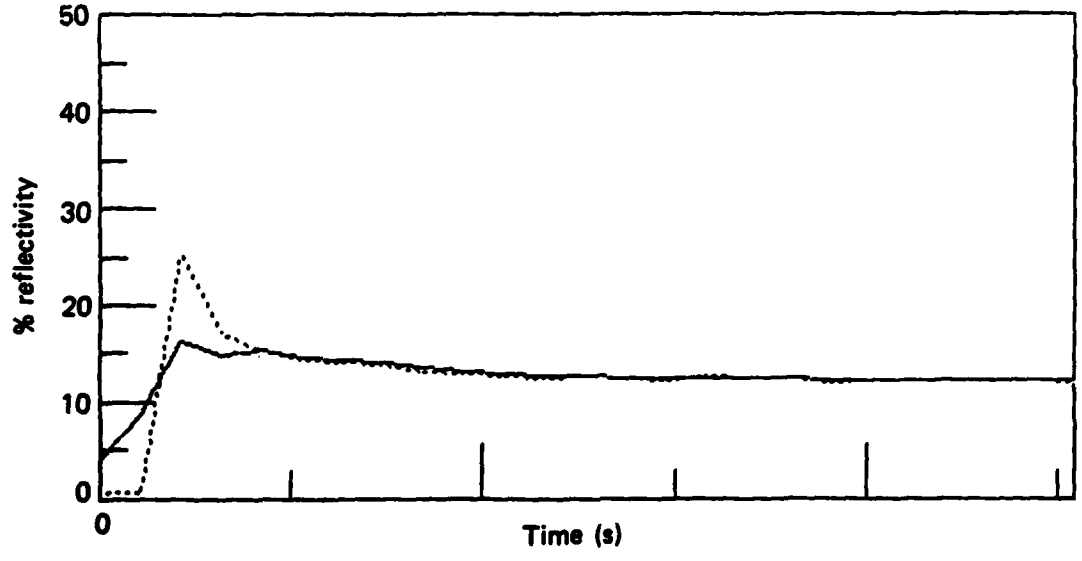


Fig. 11B

Maximum time is 127.2 s
Lambda is 658 nm

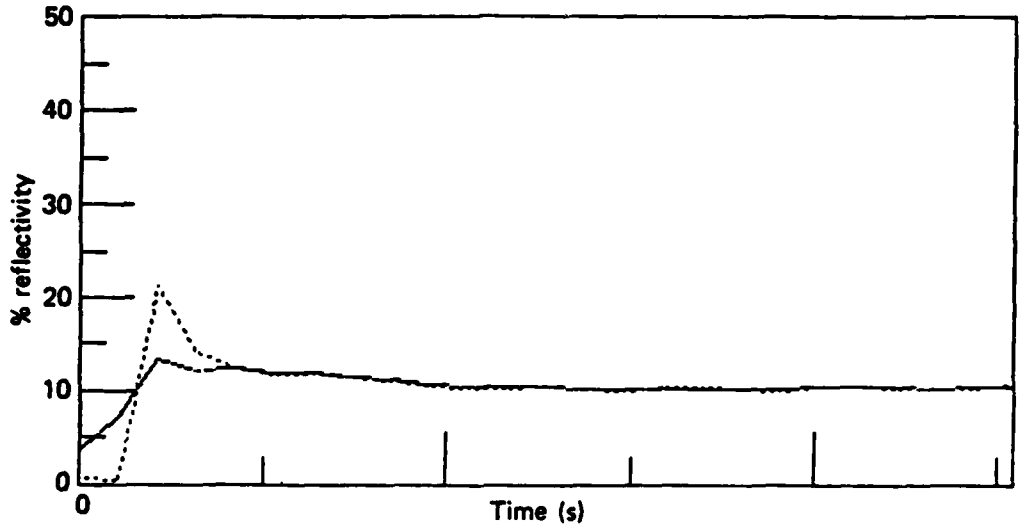


Fig. 11C

Maximum time is 127.2 s
Lambda is 695 nm

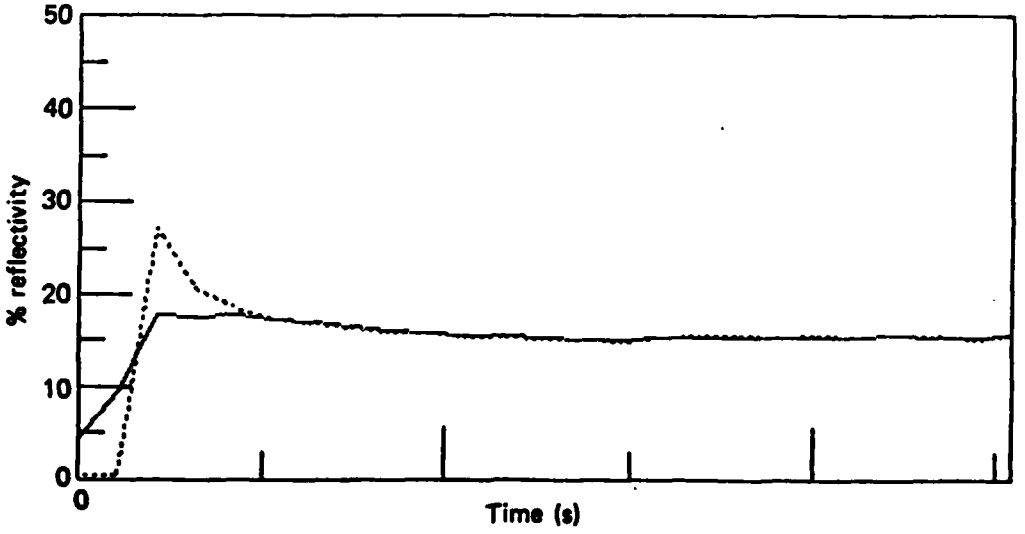


Fig. 11D

Figure 12A

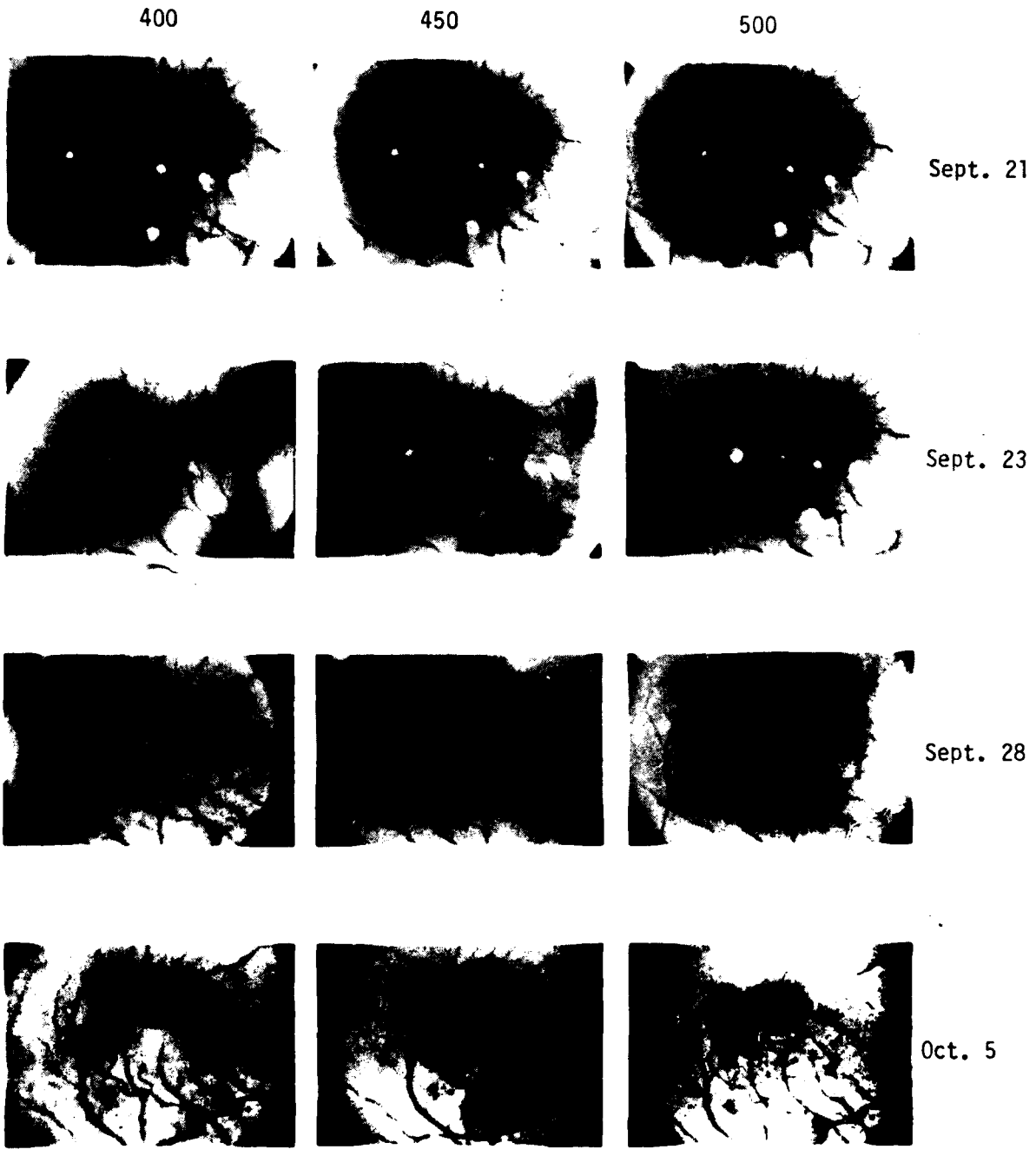

Figure 12B

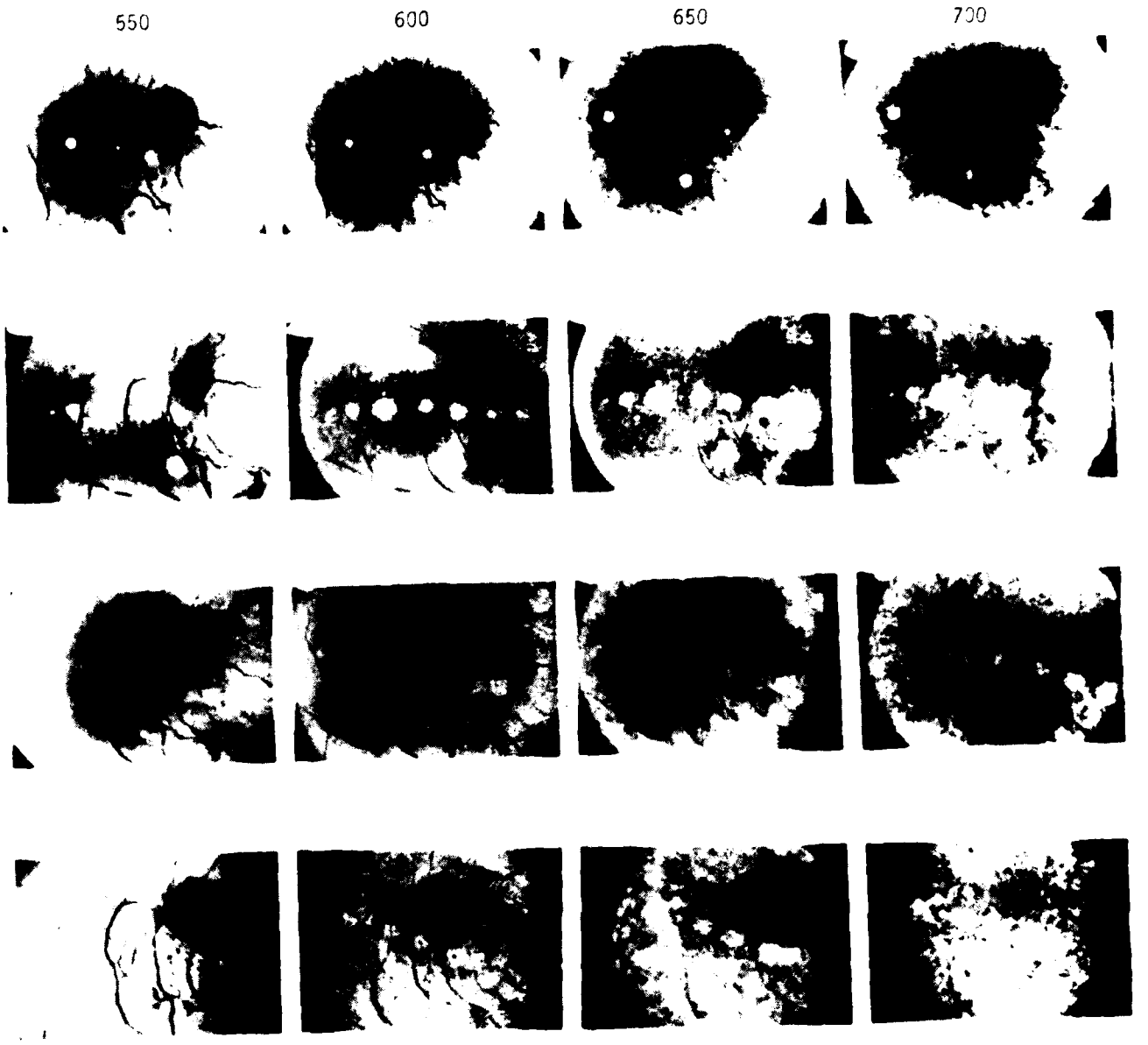

Figure 12C

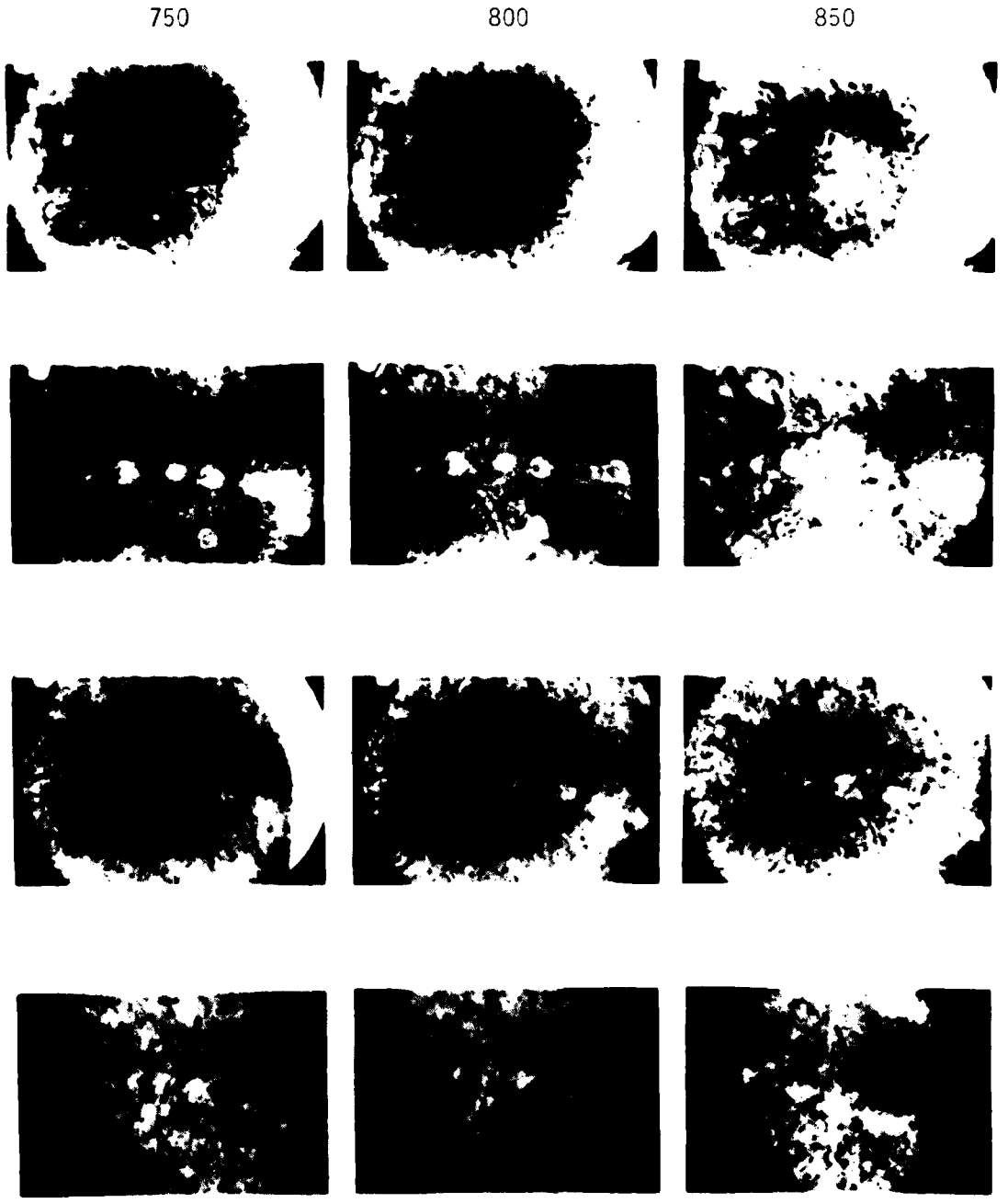

Figure 12D

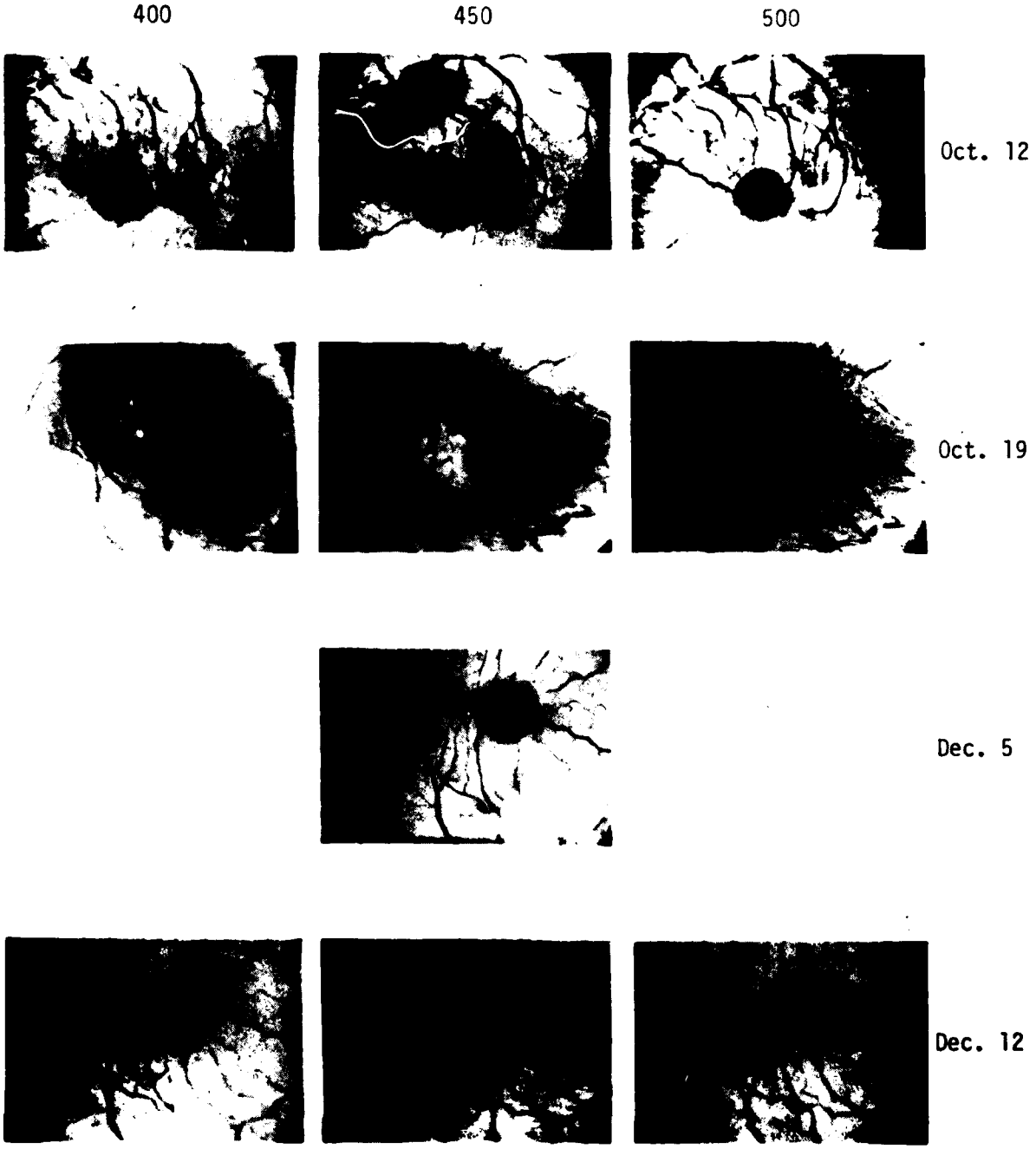

Figure 12E

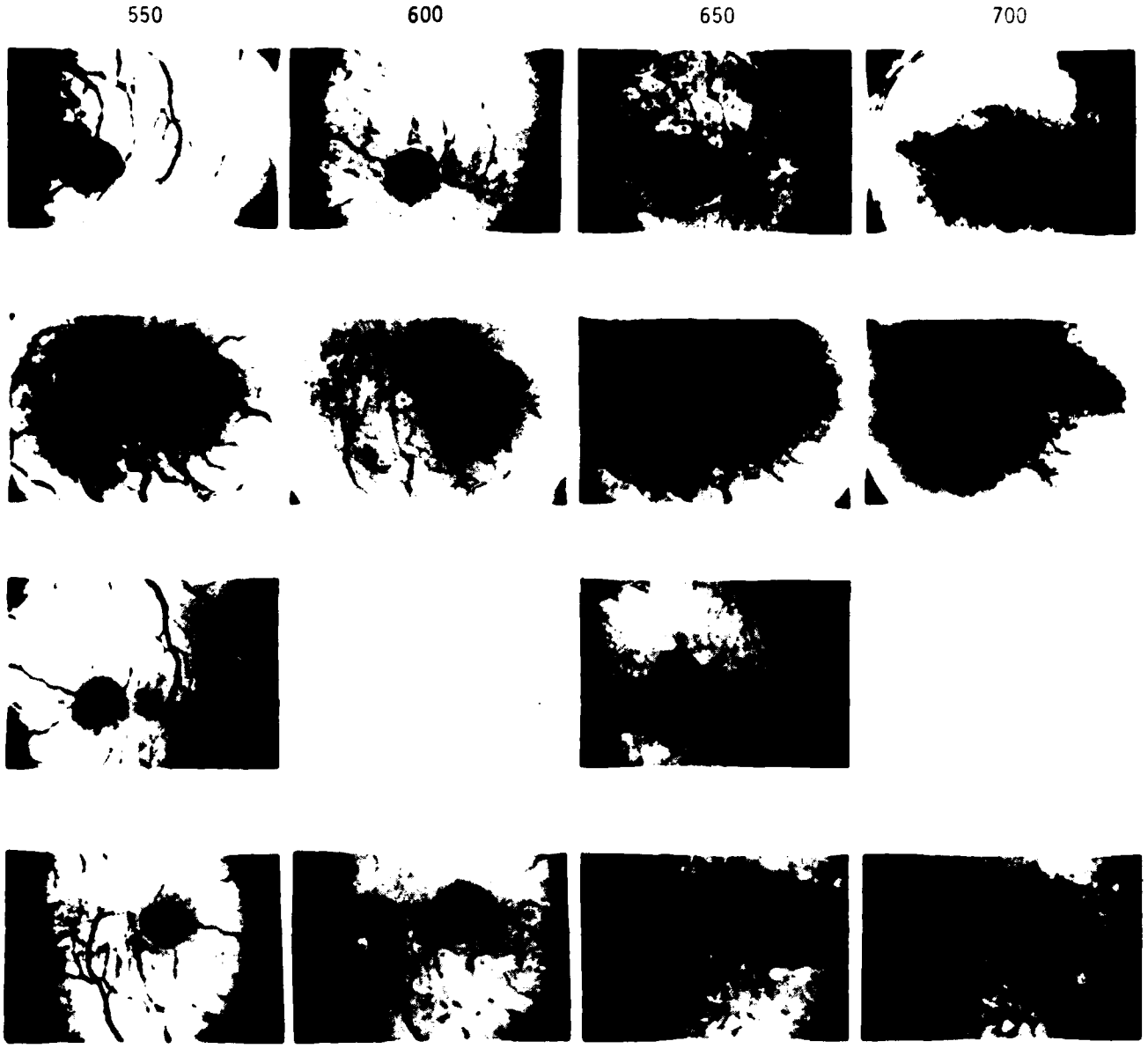

Figure 12F

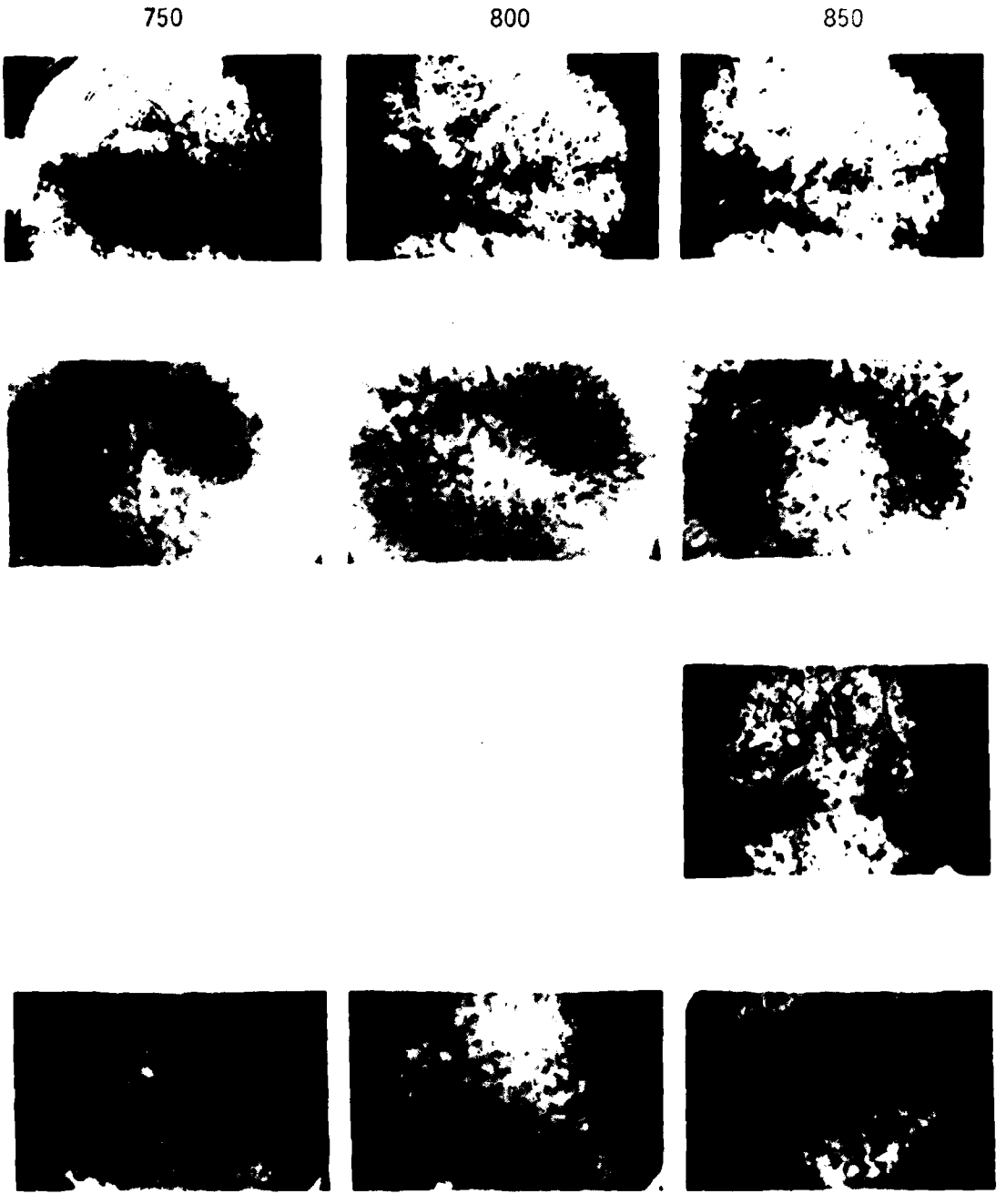

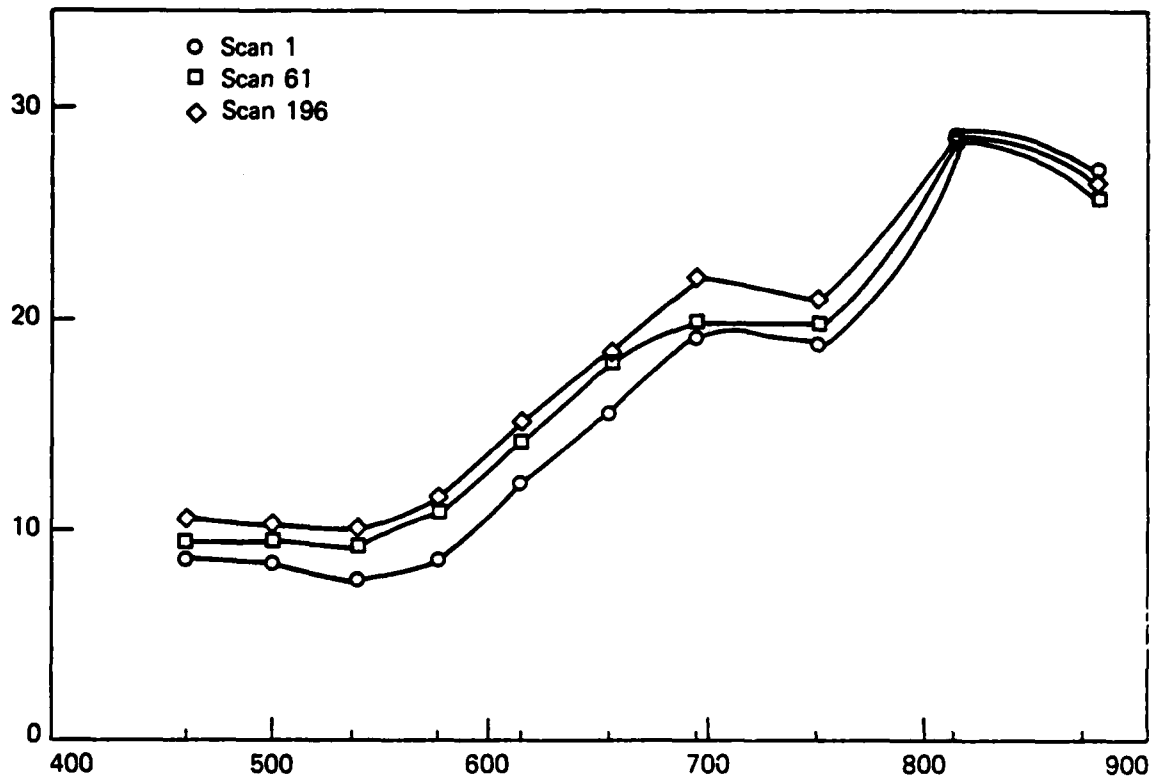
Scan 1
Scan 61
Scan 196
30
20
10
0
400
500
600
700
800
900

Fig. 13

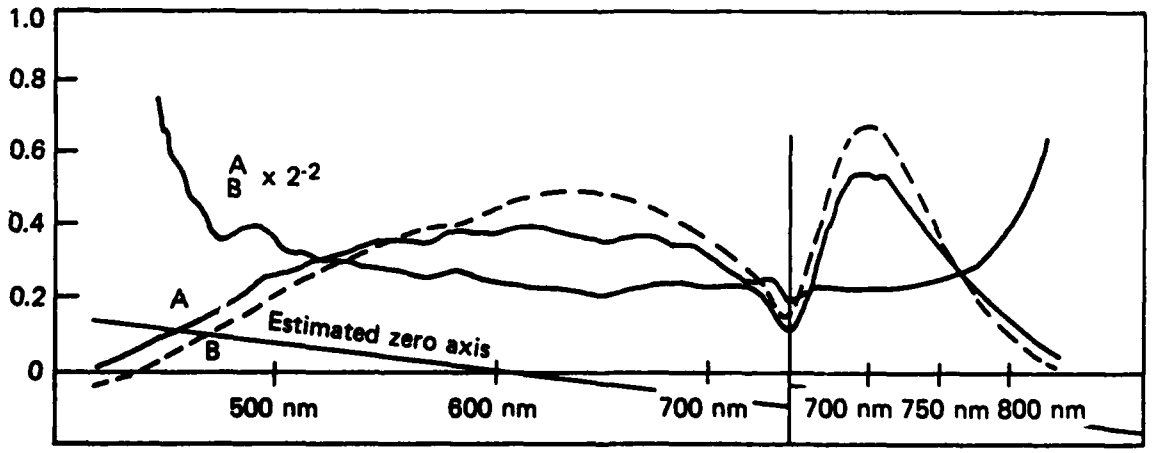
1.0
0.8
0.6
0.4
0.2
0
A/B x 2·2
A
B
Estimated zero axis
500 nm
600 nm
700 nm
700 nm 750 nm 800 nm

Fig. 14

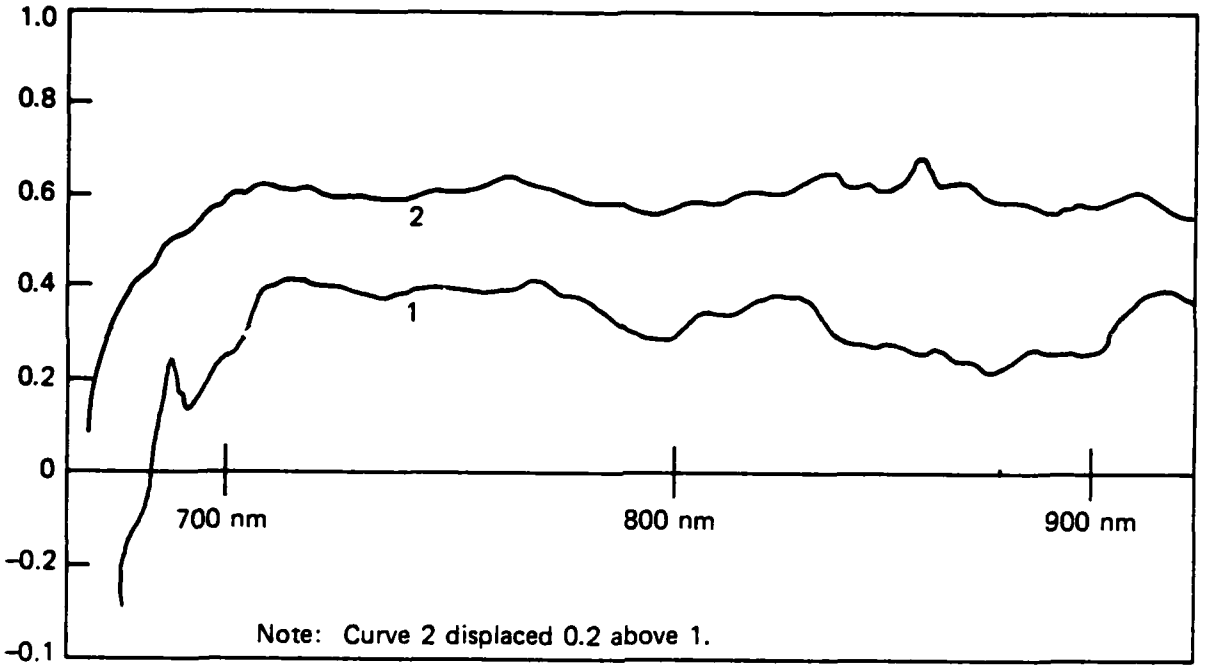
1.0
0.8
0.6
0.4
0.2
0
-0.2
-0.1
2
1
700 nm
800 nm
900 nm
Note: Curve 2 displaced 0.2 above 1.

Fig. 15

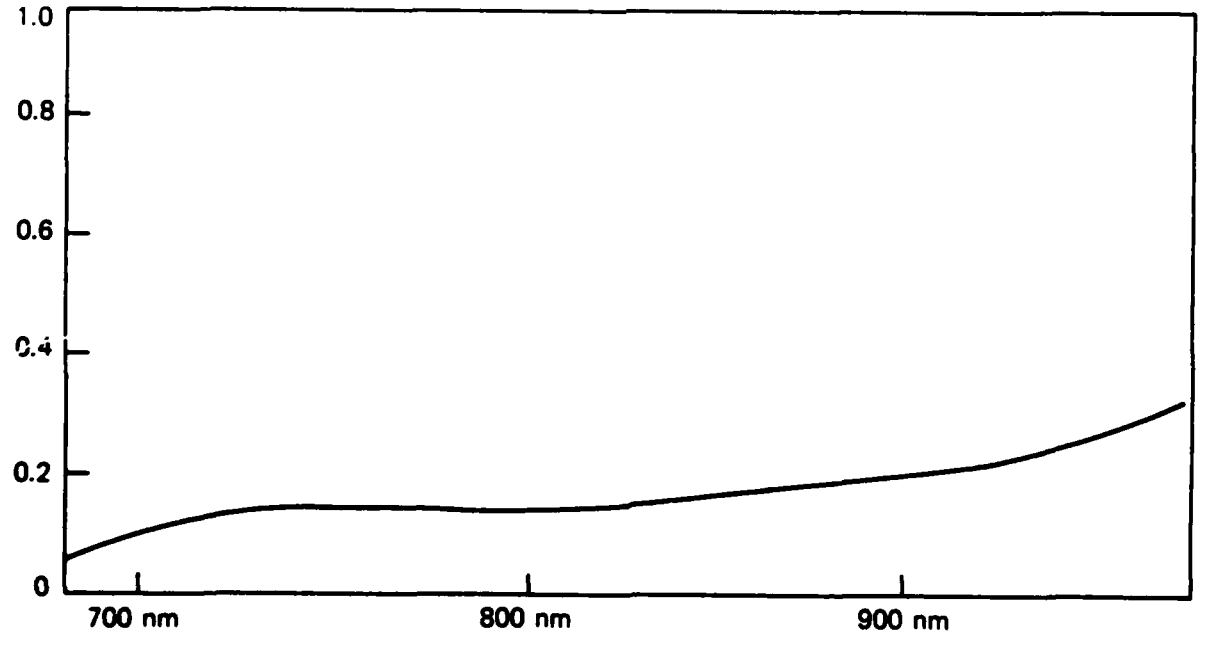
1.0
0.8
0.6
0.4
0.2
0
700 nm
800 nm
900 nm

Fig. 16